Earth-Science Reviews 197 (2019) 102916

Contents lists available at ScienceDirect

Earth-Science Reviews

journal homepage: www.elsevier.com/locate/earscirev

Planar optode: A two-dimensional imaging technique for studying spatial-temporal dynamics of solutes in sediment and soil

Cai Li[a,b], Shiming Ding[b,*], Liyuan Yang[a,*], Qingzhi Zhu[c], Musong Chen[b], Daniel C.W. Tsang[d], Gen Cai[e], Chang Feng[e], Yan Wang[b,f], Chaosheng Zhang[g]

[a] School of Water Conservancy and Environment, University of Jinan, Jinan 250022, China
[b] State Key Laboratory of Lake Science and Environment, Nanjing Institute of Geography and Limnology, Chinese Academy of Sciences, Nanjing 210008, China
[c] School of Marine and Atmospheric Sciences, Stony Brook University, New York 11794-5000, USA
[d] Department of Civil and Environmental Engineering, The Hong Kong Polytechnic University, Hung Hom, Kowloon, Hong Kong, China
[e] Institute of Optics and Electronics, Chinese Academy of Sciences, Chengdu 610000, China
[f] Nanjing EasySensor Environmental Technology Co., Ltd, Nanjing 210018, China
[g] International Network for Environment and Health, School of Geography and Archaeology & Ryan Institute, National University of Ireland, Galway, Ireland

ARTICLE INFO

Keywords:
Planar optical sensor
Biogeochemical process
High resolution sensing
Sediment quality evaluation
Sediment/soil remediation

ABSTRACT

A two-dimensional (2D) imaging technique, planar optode (PO) technique, is developed to investigate biogeochemical processes at a high resolution in heterogeneous sediments and soils, especially at the sediment-water interface. Compositional changes with depth in sediments are usually considered to be relatively steady. However, the activities of benthic organisms can generate significant heterogeneity and complex 3D transport-reaction patterns over millimeter to meter scales in the surficial sediments. Spatial and temporal quantification of the variables such as O_2 in the bioturbated sediments promoted the development of the planar optode. Different planar optode techniques including composite planar optode for multi-analytes and the combination of planar optode with diffusive gradients in thin films (DGT) have been developed and used to study the 2D solutes distributions and/or dynamics of O_2, pH, partial pressure of CO_2 (pCO_2), temperature, exoenzymes, and metal/metalloid ions in sediments and soils. New findings observed in laboratory-based microcosm experiments and field-based in situ studies using planar optode techniques, have significantly improved our understanding of heterogeneous biogeochemical reactions and processes. In this article we provide a critical review on the: 1) research progress using planar optode techniques; 2) principles, configurations, and devices used for planar optode systems; 3) characteristics and interferences associated with planar optode measurements; and 4) applications of planar optode in the environment. We have suggested the barriers, advantages, and research needs for the use of planar optodes.

1. Introduction

Obtaining data about solutes in the sediments, soils and wetlands at a high level of spatial and temporal resolution is needed to understand biogeochemical processes. Soil/sediment core slicing is a common method for studying biogeochemical processes in sediments and soils (Brendel and Luther III, 1995; Wenzel et al., 2001). Solute profiles that cannot be measured can be predicted using model calculations. However, these models are based on limited measurements and ideal assumptions, particularly for spatial and temporal monitoring. Over the past two decades, microsensors (Pedersen et al., 2015b; Revsbech, 2005), diffusive equilibration in thin films (DET) (Bottrell et al., 2007; Davison et al., 1991), high resolution dialysis (HR-Peeper) (Xu et al., 2012), and diffusive gradients in thin films (DGT) (Davison, 2016; Davison et al., 1997; Davison and Zhang, 1994) have provided analytical support for high resolution sediment and soil studies. These techniques have provided valuable insights into the ecological and biogeochemical activities of soils and sediments (Klatt et al., 2016; Li et al., 2019; Stockdale et al., 2009). However, a major limitation of microsensors is that they only allow for one-dimensional measurements (Belding et al., 2009; Lim et al., 2009), while the DGT, DET and HR-Peeper techniques require a relatively long deployment time and complex treatment processes (Ding et al., 2010, 2018; Gao et al., 2006). Furthermore, they are not suitable for the study of real-time solute transport-reaction dynamics in pore water of sediments and soils. Thus, there is a significant need for novel and robust measurement techniques

* Corresponding authors.
E-mail addresses: smding@niglas.ac.cn (S. Ding), stu_yangly@ujn.edu.cn (L. Yang).

https://doi.org/10.1016/j.earscirev.2019.102916
Received 20 February 2019; Received in revised form 2 July 2019; Accepted 26 July 2019
Available online 29 July 2019
0012-8252/

that enable non-invasive, real time, and high resolution to acquire analyte information in environment (Pascal et al., 2016; Zhu, 2019).

A simpler and more robust two-dimensional (2D) imaging technique, referred to as the planar optode (PO) technique was first developed by Glud et al. (1996), which was used to measure fine scale 2D O_2 distributions in benthic communities. The technique is based on the change of luminescence signal of specific indicator to reflect the analyte information. Since then, many different POs have been developed and used to study the 2D distributions and dynamics associated with a range of physic-chemical parameters including temperature (Borisov and Klimant, 2008a; Peng et al., 2010), pH (Hulth et al., 2002; Liebsch et al., 2001; Zhu et al., 2005), pCO_2 (Clarke et al., 2017; Schröder et al., 2007a; Zhu and Aller, 2010), ammonium (NH_4^+) (Strömberg, 2008; Strömberg and Hulth, 2005), hydrogen sulfide (H_2S) (Yin et al., 2017; Zhu and Aller, 2013), nitrate (NO_3^-) (Pedersen et al., 2015a), ferrous iron (Fe^{2+}) (Zhu and Aller, 2012), manganese (Mn^{2+}) (Soto Neira et al., 2011) and exoenzyme activity (Cao et al., 2011, 2013). POs have been introduced in real-time applications to study the sediment-water interface (SWI) (Polerecky et al., 2006; Przeslawski et al., 2009), plant rhizospheres (Blossfeld, 2013; Koop-Jakobsen et al., 2018; Larsen et al., 2015), biofilms and microbial mats (Glud et al., 1998, 1999; Moßhammer et al., 2016; Staal et al., 2011a; Vrouwenvelder et al., 2012). Composite POs have also been developed to simultaneously measure multiple analytes, including O_2/pH (Blossfeld et al., 2011; Lu et al., 2011; Meier et al., 2011), O_2/pCO_2 (Borisov et al., 2006; Schröder et al., 2007a), O_2/temperature (Stich et al., 2008; Zelelow et al., 2003), O_2/pH/temperature (Stich et al., 2010b) and O_2/pCO_2/pH/temperature (Borisov et al., 2011). In addition, the PO-DGT composite sensors are integrated, by combining the PO sensing layer with DGT binding gel, which is a promising development that can provide researchers with new insights in different biogeochemical processes at the micro scale (e.g., mineral formation and uptake by biota). PO-DGT has been applied to perform the 2D imaging of O_2 and trace metals and phosphorus dynamics in sediments (Han et al., 2017; Lehto et al., 2017; Stahl et al., 2012), and to study pH and multiple metals in rhizospheres (Hoefer et al., 2017).

This paper provides a comprehensive review on principles, available system configurations and devices, related performances and applications of planar optodes and their combination with the DGT technique. Some of the problems with planar optodes, which are not often considered by scientists are discussed in detail (e.g., the wall effect and the effects of light scattering particles). Furthermore, the challenges, future development directions and potential applications of planar optodes are presented.

2. The imaging principles and methods of planar optode

Most solutes in sediments or soils are colorless/non-fluorescent and cannot be directly determined using optical methods; thus, a luminescent transducer is needed to convert analyte concentrations into a measurable optical signal. Based on analyte characteristics, analyte-sensitive indicators can be immobilized in a thin layer of analyte-permeable polymer matrix. Analyte diffuses into the matrix and interacts with the immobilized indicators, and then the indicators are excited by light sources and emitting light signals, which are recorded by charge coupled device (CCD)/digital camera (Fig. 1). Analyte concentration is quantified using the changes in the luminescence intensity or lifetime. The principle of the planar optode measurement is based on changes in luminescence intensity, lifetime and/or absorbance of the optical transducer (Table 1). The intensity-based imaging includes pure intensity, wavelength ratiometric, and color ratiometric measurements. Lifetime-based imaging involves time domain (TD) lifetime imaging (rapid lifetime determination (RLD), time domain dual lifetime referencing (t-DLR)) and frequency domain (FD) lifetime imaging.

2.1. Luminescence intensity-based imaging

2.1.1. Pure luminescence intensity imaging

Pure luminescence intensity measurement has been widely applied in PO imaging, based on the luminescence intensity change of a single luminescent indicator (Choi and Hawkins, 2003; Konig et al., 2005). The normal Stern-Volmer equation is often utilized for luminescence quenching-based optical sensors:

$$\frac{I}{I_0} = 1 + K_{sv}C \tag{1}$$

where I and I_0 is the luminescence intensity in the presence and absence of analytes, respectively; K_{sv} is the Stern-Volmer quenching constant; and C is the analyte concentration. Several planar optodes have utilized the normal Stern-Volmer equation to describe the relationship of analytes concentration and luminescence intensity, such as the optodes of O_2, H_2S and CO_2 (Choi and Hawkins, 2003; He and Rechnitz, 1995; Schröder et al., 2007a; Zhu and Aller, 2013).

However, a non-linear response was presented in planar optodes due to polymer-supported sensors exhibited a degree of heterogeneity, compared with the ideal fluid solution system, especially the O_2 planar optode. Therefore, a more realistic two-site model includes quenching at two heterogeneous sites was introduced to describe the nonlinear Stern-Volmer quenching behavior (Borisov et al., 2011; Carraway et al., 1991; Demas et al., 1995; Stich et al., 2008):

$$\frac{F}{F_0} = \frac{\tau}{\tau_0} = \frac{\alpha}{1 + K_{sv1}[O_2]} + \frac{1-\alpha}{1 + K_{sv2}[O_2]} \tag{2}$$

Where α is the non-quenchable fraction; K_{sv1} and K_{sv2} is the Stern-Volmer quenching constant of two sites, respectively; and $[O_2]$ is the O_2 concentration. The two-site model assumes the existence of two different microenvironments with substantially different accessibility for oxygen (Borisov et al., 2012). In some case, if one site of the immobilized luminescent indicator is non-quenchable (inaccessible for O_2), the K_{sv1} could be set as 0, the two-site model can be simplified to a modified Stern-Volmer equation (Klimant et al., 1995; Koren et al., 2019):

$$\frac{F}{F_0} = \frac{R}{R_0} = \frac{\tau}{\tau_0} = \alpha + (1-\alpha)\left(\frac{1}{1 + K_{sv}[O_2]}\right) \tag{3}$$

where F and F_0 are the fluorescence intensity in the presence and absence of O_2, respectively; α is the non-quenchable fraction of the fluorescence; and $[O_2]$ is the O_2 concentration. For a given mixture of luminescent indicators and matrix materials, α is temperature independent and constant in the dynamic range of the optode (Kühl, 2005). Therefore, once α has been determined (α can be determined using at least three different O_2 concentrations), O_2 planar optodes can be calibrated by a simple two-point calibration at experimental condition.

2.1.2. Wavelength ratiometric imaging

Wavelength ratiometric imaging is the other method of intensity-based imaging, which relies on two different excitation wavelengths, or two different emission wavelengths, or dual-excitation dual-emission of luminescent indicators (Hulth et al., 2002; Song et al., 1997; Strömberg and Hulth, 2003; Strömberg et al., 2009b). Zhu et al. (2005, 2006b) developed a pH optode using 8-Hydroxypyrene-1, 3, 6-trisulfonic acid trisodium salt (HPTS) which was covalently immobilized on surface of polyvinyl alcohol (PVA) membrane. This pH shows fluorescence emission at 540 nm but dual excitation at 428 and 506 nm for the acid and base forms of HPTS, respectively. The RGB (red, green, blue) color image obtained at 540 nm, the intensity ratio σ of green channel emission intensities excited at 506 to that excited at 428 nm are applied to pH calculation (Kermis et al., 2002):

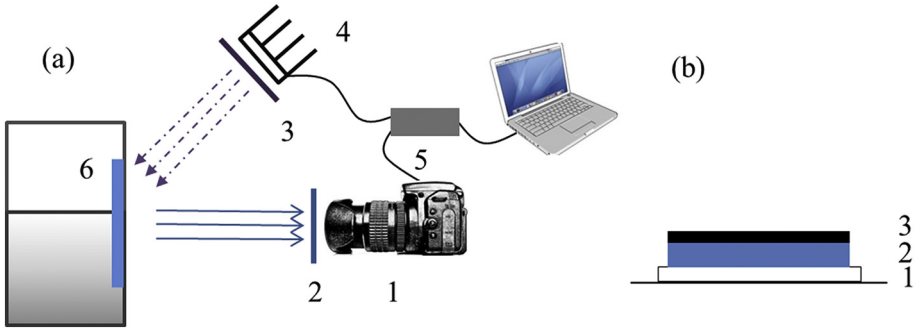

Fig. 1. (a) PO systems: 1 camera; 2, 3 optical filters; 4 excitation light source; 5 trigger unit; 6 PO; (b) PO structure: 1 support material; 2 sensing layer; 3 optical insulation layer.

$$\mathrm{pH} = \mathrm{p}K_a' - \log\frac{(\sigma_{max}-\sigma)}{(\sigma-\sigma_{min})} - \log\frac{(\varepsilon_{PTS^-}\varnothing_{PTS^-})\lambda_2}{(\varepsilon_{HPTS}\varnothing_{HPTS})\lambda_2} \quad (4)$$

where $\sigma_{\min}$ and σ_{max} are the ratio at the most acidic and basic ends of the working range where total HPTS is dominated by HPTS and PTS^-, respectively. The ε_{PTS^-}, $\varnothing_{PTS^-}$ are the extinction coefficient and quantum yield of PTS^- at the base form excitation maximum λ_2; and ε_{HPTS}, $\varnothing_{HPTS}$ are the extinction coefficient and quantum yield of HPTS at the excitation maximum λ_2, respectively. The K_a' value is the dissociation constant of HPTS.

Based on the similar optical transduction principle, the 2D pCO_2 distribution in marine sediments was also determined using the pH indicator HPTS immobilized within an ethyl cellulose membrane, which has single fluorescence emission maximum at 515 nm with dual excitation at 405 nm and 475 nm for the acid and base form of HPTS, respectively (Zhu and Aller, 2010; Zhu et al., 2006a). Therefore, the pCO_2 can be calculated by the intensity ratio R of fluorescence intensity (green channel) at 515 nm excited at 475 to that excited at 405 nm:

$$pCO_2 = \frac{k'}{R} - k'' \quad (5)$$

where k' and k'' are constant.

In addition, wavelength ratiometric imaging method has been applied to measure ammonium/ammonia. This procedure relies on the solvent sensitive or solvatochromic compound, merocyanine 540 (MC 540), which has optical characteristics that change excitation/emission fluorescence properties upon shift of solvent (ex. 510 nm, em.568 nm fluorescence in the hydrogel phase; ex.568, em.589 nm fluorescence in the ether phase) (Strömberg and Hakonen, 2011; Strömberg and Hulth, 2006). Therefore, the ammonia concentration $[NH_3]$ can be quantified using the intensity ratio R ether fluorescence/hydrogel fluorescence (568 nm:589 nm/510 nm:568 nm):

Table 1
Overview of PO imaging approaches.

Imaging method		Analytes	Remark	References
Luminescence intensity-based imaging	PI[a]	Enzyme O_2 H_2S pH	Simple imaging approach, vulnerable to background interference.	Cao et al. (2011), Pischedda et al. (2010), Rudolph et al. (2011, 2017), Song et al. (2012), Zhu and Aller, 2013
	WR[b]	pH pCO_2 NH_3	Simple imaging approach, insensitive to background interference and uneven distribution of indicators	Hakonen et al. (2010), Strömberg (2008), Strömberg and Hulth (2005), Zhu and Aller (2010), Zhu et al. (2006a, 2006b)
	CR[c]	pH O_2 NH_3 pCO_2	Simple imaging approach vulnerable to background interference	Blossfeld et al. (2013), Jiang et al. (2017b), Moßhammer et al. (2016), Tobias et al. (2012)
Luminescence lifetime-based imaging	RLD[d]	Temperature O_2 pH pCO_2	Insensitive to background interference and photobleaching, luminescent indicators degradation, but need expensive and fast gateable CCD camera, home-made triggering systems and software	Borisov and Klimant (2008a), Konig et al. (2005), Liebsch et al. (2000), Murniati et al. (2016)
	t-DLR[e]	pH O_2 pCO_2 Temperature		Borisov et al. (2011), Liebsch et al. (2001), Schröder et al. (2007a), Stahl et al. (2006)
	RLD + t-DLR	pH Temperature O_2		Schröder et al. (2007b), Wang et al. (2012)
	FD[f]	O_2 pCO_2	Insensitive to background light, but vulnerable to the background fluorescence	Borisov et al. (2006), Franke and Holst (2015), Koren et al. (2019)
Absorbance- based imaging	Abs[g]	Fe^{2+} Mn^{2+} H_2S	Simple imaging setups, only use inexpensive standard flatbed scanner	Soto Neira et al. (2011), Yin et al. (2017), Zhu and Aller (2012)

[a] Pure intensity.
[b] Wavelength ratiometric.
[c] Color ratiometric.
[d] Rapid lifetime determination.
[e] Time domain dual lifetime referencing.
[f] Frequency domain.
[g] Absorbance.

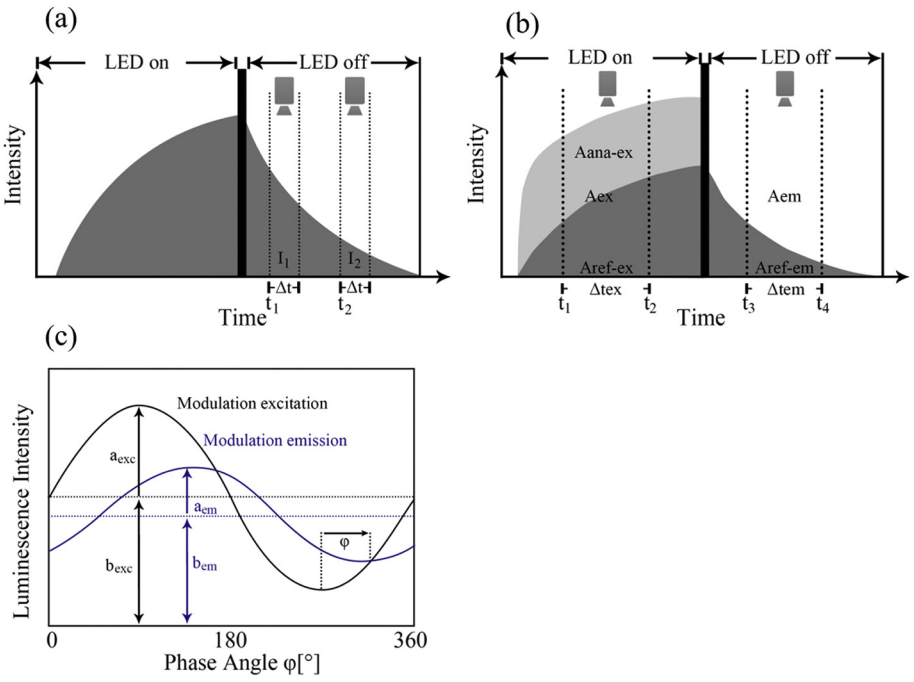

Fig. 2. Luminescence lifetime-based imaging approaches: (a) Rapid lifetime determination (RLD), the lifetime τ is determined by measuring two integrated intensities (I_1 and I_2) over a time-window of equal width ($\triangle t$) at two points t_1 and t_2 separated by time difference (t_2–t_1). (b) Time domain dual lifetime referencing (t-DLR), two images are taken at two time periods, during the excitation phase (t_1–t_2) where analyte-sensitive and reference indicators emit ($A_{ex} = A_{ana\text{-}ex} + A_{ref\text{-}ex}$) and during the decay phase (t_3–t_4) where only the reference indicator emits ($A_{em} = A_{ref\text{-}em}$). Modified from Schröder et al. (2007a). (c) Frequency domain (FD) luminescence lifetime, Luminescence is photoexcited with sinusoidally modulated light (black trace), and the luminescence of the indicator probe (blue trace), but phase-shifted by an angle, φ. Modified from Koren et al. (2019). (For interpretation of the references to color in this figure legend, the reader is referred to the web version of this article.)

$$R = \alpha\sqrt{[NH_3]} + R_0 \quad (6)$$

where R and R_0 is the fluorescence ratio in the presence and absence of NH_3 respectively; and α is a constant determining the slope of the function.

2.1.3. Color ratiometric imaging

Color ratiometric imaging is a relatively simple and inexpensive setup that requires a built-in color filter in the camera to record color image. The color image is split into red, green and blue or near infrared (NIR) channels, and the intensity ratio of different color channels are then used to determine the analyte concentrations. The different color channels are dominated by different luminescent indicators (e.g. the analyte-sensitive dyes and reference or donor dyes). Color ratiometric imaging has been used to measure O_2 distributions and dynamics. The calibration curve for O_2 optodes fit a modified Stern-Volmer equation Eq. (3), where, R and R_0 represent the pixel intensity ratio of different color channel in the presence and absence of O_2, respectively. The variable R depends on the characteristics of the O_2-sensitive indicator and reference or donor indicator. Larsen et al. (2011) selected red channels of PtOEP as the indicator; the green channels of Macrolex yellow coumarin served as an internal reference. Other researchers used the color ratiometric imaging setup (Christel et al., 2016; Haas et al., 2013):

$$R = \frac{Red - Green}{Green} \quad (7)$$

In addition, Jiang et al. (2017a) used the intensity ratio of the red channels of the O_2 indicator PtOEP and the blue channels of reference quantum dots (QDs) ($R = Red/Blue$) to measure O_2 distribution. The intensity ratios of the red channels of the O_2 indicator europium complex (Eu(HPhN)$_3$dpp) and the green channels of the reference coumarin dye (Bu$_3$Coum) ($R = Red/green$) have also been used (Moßhammer et al., 2016).

Based on the color ratiometric imaging, the calibration curve of pH optodes can be described using a sigmoidal curve with 4 fitting parameters (Larsen et al., 2011):

$$\mathrm{R} = R_0 + \frac{a}{1 + e^{-(pH - pK_a)/b}} \quad (8)$$

where a, b are fitting constants, with a expressing the asymptotic values at low and high pH, b expressing the slope around pK_a. The variable pK_a is the inflection point of the curve (acid dissociation constant). The variable R and R_0 represent the pixel intensity ratio or fluorescence intensity at different pH values and at the lowest pH values within standard curve, respectively. The intensity ratio R of the NIR channels of the pH indicator (OHButoxy-aza-BODIPY) to the green channels of the reference coumarin dye (Bu$_3$Coum) ($R = NIR/Green$), the green channels of the the pH indicator (5-Fluorescein) to the blue channels of the reference quantum dots (QDs) ($R = Green/Blue$) have been applied to obtain the pH calibration curve (Jiang et al., 2017a; Moßhammer et al., 2016). These calibration parameters are determined using 6–10 points calibration that accounts for the expected pH range.

2.2. Lifetime-based imaging

Lifetime imaging is a robust method, where the luminescence decay time of phosphorescence is recorded by using a fast flashlamp and gateable CCD camera. Combining the rapid lifetime determination (RLD) with the transparent oxygen optode allows an initial simultaneous investigation of the 2D distribution of O_2 and sediment physical structure (Holst and Grunwald, 2001). The RLD method has also been used to study the distributions of O_2, pH and CO_2 (Hartmann and Ziegler, 1996; Holst et al., 1998; Liebsch et al., 2000). Especially, the O_2 optodes often be calibrated using the RLD method, based on the modified Stern-Volmer equation Eq. (3) (Glud et al., 2016; Jovanovic et al., 2014), where τ and τ_0 represent the luminescence lifetime in the presence and absence of O_2, respectively. The lifetime τ is determined by measuring two integrated intensities (I_1 and I_2) over a time-window of equal width ($\triangle t$) at two points t_1 and t_2 separated by time difference ($t_2 - t_1$) (Fig. 2a) (Grauw and Gerritsen, 2001; Liebsch et al., 2000; Murniati et al., 2016):

$$\tau = \frac{t_2 - t_1}{\ln \frac{I_1}{I_2}} \quad (9)$$

Time domain dual lifetime referencing (t-DLR) as a relatively simple method has been applied for planar optode imaging, especially those luminescent indicators with decay times of < 100 ns (Borisov et al., 2011; Liebsch et al., 2001; Stich et al., 2010a). The t-DLR imaging

approach is based on the acquisition of two images (Fig. 2b). One image (A_{ex}) is collected during the excitation period, when the light source is on (the sum of luminescence intensity of both the analyte sensitive fluorescence (A_{ana-ex}) and the analyte insensitive phosphorescence (A_{ref-ex})). The second image (A_{em}) is collected during decay period, when the light source is off (the intensity of the analyte insensitive phosphorescence (A_{ref-em})). The ratio of the images provides a reference intensity distribution that reflects the analytes information at each pixel, and t-DLR method has been applied the pH and CO_2 imaging (Schröder et al., 2005, 2007a, 2007b; Stahl et al., 2006). The luminescence ratio $R = A_{ex}/A_{em}$ and pH is also suitable for a sigmoidal curve (Eq. (8)) (Liebsch et al., 2001; Stahl et al., 2006):

$$R = \frac{A_{ex}}{A_{em}} = \frac{A_{ref-ex} + A_{ana-ex}}{A_{ref-em}} \tag{10}$$

Frequency domain luminescence lifetime imaging has been also well established to measure the lifetime of luminescent indicators. As shown in Fig. 2c, the luminescent indicator is excited using sinusoidally modulated light, and luminescence emission of indicator is sinusoidally modulated as well, but phase-shifted by an angle, φ (Franke and Holst, 2015; Wang and Wolfbeis, 2014). In case of single exponential decay, the phase angle of the luminescent signal modulated at a single modulation frequency f_{mod} reflects the decay time τ of the luminescent indicator (Ogurtsov and Papkovsky, 1998):

$$\tan(\Phi) = 2\pi f_{mod}\tau \tag{11}$$

The frequency domain luminescence lifetime imaging has been demonstrated to be a robust and simple chemical imaging method for planar optode imaging, and shown to be well application in sediments (Koren et al., 2019).

2.3. Absorbance-based imaging

Some planar optical sensors based on UV-VIS absorbance have been developed to measure 2D distribution of various analytes. The planar optical sensor was directly inserted into the soils or sediment, which allow reacting with analytes in relatively short time (typically minutes). The planar optical sensor was then retrieved and simply rinsed, finally was imaged using inexpensively standard flatbed scanner (Zhu, 2019). Yin et al. (2017) constructed a novel irreversible H_2S sensor by using the DPCO-Zn^{2+} complex entrapped in a transparent polymer layer coated on a polyester matrix. The absorbance change ($\Delta A = A_0 - A$, A_0 is blank sensor absorbance without H_2S and A is sensor absorbance with H_2S) of the DPCO-Zn^{2+} complex decreased with an increased in H_2S concentration; there was also a good linearity in the sensor response (ΔA) at low H_2S concentrations. In addition, 2D distributions of Fe^{2+} in marine sediments was measured using a sensor which Ferrozine was covalently immobilized onto a transparent poly (vinyl alcohol) membrane backed by a polyester sheet (Zhu and Aller, 2012). The absorbance of sensor increased with an increase in Fe^{2+} concentration; there was an excellent linear relationship between absorbance and Fe^{2+} concentrations in the range of 0–200 μM.

2.4. Advantages and disadvantages of various imaging methods

Pure intensity-based imaging approaches do not require sophisticated equipment and tedious image processing. However, these techniques are sensitive to changes in background reflection, external excitation light sources and factors associated with the sensing membrane (e.g. heterogeneous distribution of the luminescent indicators in the sensing membrane) and illumination by the source. To some extent, these interferences can be reduced by carefully pixel-to-pixel calibrating the optodes before and after use, or by covering the optical isolation layer lying on top of the sensing layer (Glud et al., 1996; Strömberg and Hulth, 2005). Compared to the pure intensity imaging method, wavelength ratiometric measurements are relatively insensitive to heterogeneous distributions of luminescent indicators and fluctuation of excitation light. Furthermore, wavelength ratiometric measurements can significantly minimize or eliminate the interference from background reflectance (Zhu et al., 2006b). The color ratiometric imaging makes it possible to simultaneously measure multiple analytes using a single sensor (Larsen et al., 2011; Moßhammer et al., 2016). However, this method is sensitive to color-dependent light scattering from the soil or sediment behind the optode. Some studies have utilized an opaque membrane or a semi-transparent layer of silicone as an optical insulation layer to reduce this interference (Larsen et al., 2011). However, the use of these optical insulation layers can increase the response time, which limits the study of sediments or soils with inherently fast dynamics. Research suggests that the t_{90} response time (time to reach 90% of the full signal) of an O_2 optode with a silicone layer is ~ 10 times higher than tan optode without the silicone layer (Larsen et al., 2011). Insulation of the sensor, using silicone or other insulating materials can obstruct structures behind the sensor, making it cumbersome to assess the relative position of the sediment-water interface (SWI), rhizosphere or related anomalies in the sediment structure.

Lifetime-based imaging is often more accurate and stable than intensity-based imaging. This is independent of interference due to heterogeneous illumination, photobleaching, luminescent indicators degradation, or background interference signals (Borisov et al., 2012; Holst et al., 1998). Furthermore, the lifetime-based imaging can measure multiple analytes simultaneously by combining RLD and t-DLR imaging method (Schröder et al., 2007a; Wang et al., 2012). In case where luminescent signals and background interference signals have different decay time, lifetime imaging (μs) can be used to eliminate the background interference signals (ns). Therefore, luminescent indicators with relatively long lifetimes (> 1 μs) are best to use in lifetime imaging (Borisov et al., 2010). Some studies have used TiO_2 micro-particles in lifetime imaging to help meet the strict requirements of this technique (e.g., helping enhance phosphorescence intensity and increase the lifetimes of differential luminescent indicators) (Chatni et al., 2009). However, these particles scatter light and thus carry a potential risk of reducing spatial resolution (see Section 3.4). Koren et al. (2019) compared the performances and characteristics of time domain and frequency domain lifetime imaging. Similar calibration curves and O_2 distributions in the rhizosphere were observed, but the frequency domain camera system showed slightly better imaging quality. On the other hand, frequency domain lifetime imaging is not susceptible to the weak external background light such as turned away desk-lamps or nearby aquaria lights, but it is vulnerable to the background fluorescence (e.g. chlorophyll or other photopigments). The major disadvantages associated with the use of lifetime-based imaging are: (1) lifetime-based imaging requires a more sophisticated, expensive camera system, home-made triggering systems and software; (2) lifetime-based imaging involves the division of two or more images, which can result in considerably higher noise within the analytical signal (lifetime), reducing the precision.

Planar optodes based on absorbance imaging are often irreversible, one-shot irreversible planar sensors that cannot be used to measure solute dynamics. However, they are particularly useful for resolving complex 3D patterns of solute concentrations and relating these patterns back to the biogenic structures in marine sediments. Recent studies have found that this technique is particularly effective when sensor plates are deployed in marine sediments at regularly spaced intervals (e.g. 1–2 cm apart) (Zhu et al., unpublished data). These sensor plates have been found to be able to define successive vertical 2D sections, and by using image processing software (e.g. Image J) to superimpose these 2D images, delivering a 3D construction of the desired sediment area (Yin et al., 2017).

3. Planar optode sensor

The PO sensor sheet includes an immobilized optical indicator in a polymer membrane, supported by a transparent plastic sheet. It typically consists of three layers: a transparent support sheet, a sensing polymer membrane, and an optical insulation layer or protective layer.

3.1. Support sheet

The support sheet mainly serves as a physical holder to support and hold the soft sensing polymer membrane. The support sheet must be transparent, resistant to organic solvents, and convenient for fabrication, transport, handling and deployment of sensor membrane. The most frequently used support sheet is a dust free polyester support foil (PET) (Glud et al., 1996, 1998; Jiang et al., 2017a). Other transparent materials may be used, if they are resistant to the matrix solvent and inert towards the indicators, such as glass support (Fischer and Wenzhöfer, 2010; Kuhl et al., 2007; Wang et al., 2010). Some studies have tested the spatial resolution of the PO setup using a resolution test target (USAF 1951 resolution target). The results have shown that the practical spatial resolution is less than the theoretical maximum resolution of the camera image sensor (Larsen et al., 2011; Strömberg and Hulth, 2005). The image distortion was possibly caused by light being guided into the support layer and the (aquarium) walls. Fischer and Wenzhöfer (2010) used a fiber optic faceplate (FOFP) coated with indicator dye, which ensured that the light could only travel in a straight line in each single fiber. The use of FOFP can significantly reduce optical cross-talk and enhance the maximal spatial resolution that can be achieved with planar optode measurements (Bachar et al., 2008; Lehto et al., 2017). Mayr et al. (2012) proposed a simple approach for coating the additional optical filter layer at the bottom of the support sheet, with the optical filter layer absorbing the cross-talk light to a higher extent than the virtual signal, allowing for suppressing the optical cross-talk effects.

3.2. Sensing membrane

The sensing membrane is a key component of planar optode, and determines sensor characteristics including sensitivity, selectivity, dynamic range, response time and sensor stability. The indicator, reference dye, polymer matrix, and some light-scattering particles are integrated into a solid polymer layer to facilitate sensor interaction with the solutes in the water medium.

3.2.1. Polymer matrix

Suitable polymer matrixes are essential for performances of planar optodes, including analyte-permeability, response time, sensitivity, chemical stability, dynamic range and tolerance to the environmental interferences (Courbat et al., 2009; Koren et al., 2013; Wolfbeis, 2005). The frequently used polymer matrixes in planar optodes, as well as their suitable analytes and physicochemical characteristics were summarized in Table 2. Polystyrene (PS) and its derivatives, ethyl cellulose (EC), plasticized poly (vinyl chloride) (PVC), sol-gel, polydimethylsiloxane (PDMS), and polymethyl methacrylate (PMMA) are gas permeable. Therefore, they are often used in the measurement of dissolved gasous analytes such as O_2, CO_2 and H_2S (Glud et al., 1996; Precht et al., 2004; Zhu and Aller, 2013; Zhu et al., 2006a). PDMS, PS and PMMA matrixes are completely ion-impermeable polymer matrices which can effectively decrease the cross-sensitivity to ions strength and protons. Compared with the PDMS and PS, PMMA has relative lower O_2 permeability, and it is only useful for sensing O_2 at high partial pressure (Wang and Wolfbeis, 2014). PS has been the most common O_2 polymer matrix due to its moderate oxygen permeability, good chemical stability and mechanical properties, as well as compatibility with most O_2 indicators (Borisov et al., 2014). Koren et al. (2013) evaluated the effects of different polystyrene-derivatives polymer matrixes on the dynamic range and sensitivity of O_2 planar optodes. The results indicated that the sensitivity of O_2 planar optode was related to the spacing between the polymer strands and void volume. tButPS matrixes can increase the void volume in polymer matrix which dramatically improved the sensitivity of O_2 planar optodes, compared with PS and other polystyrene-derivatives. In addition, the working range of O_2 planar optode can be tuned using different polystyrene-derivatives although using the same indicator (Koren et al., 2013), and this make it feasible to customize the sensor response range based on practical application and sensing environments.

HydroMed D4 is an ether-based hydrophilic urethane that has excellent adhesive and cohesive properties. It is optically transparent and mechanically robust, and is highly permeable for gas, water and protons. These characteristics make it suitable for the determination of pH, O_2, H_2S, NO_3^- and extracellular enzyme activity (Cao et al., 2013; Pedersen et al., 2015a; Schröder et al., 2007b; Yin et al., 2017). Furthermore, HydroMed D4 is also used as the immobilization matrix for planar optodes based on optical microparticles or nanoparticles, due to its high permeability for various analytes (Borisov et al., 2006; Meier et al., 2011). Poly (vinyl alcohol) (PVA), high molecular weight PVC as well as poly(acrylonitrile) (PAN) have been applied to be polymer matrixes to design the temperature optodes by using O_2-sensitive indicators, due to their low gas permeability (Liebsch et al., 1999; Peng et al., 2010; Stich et al., 2008). Furthermore, some luminescent indicators can be covalent bond on the PVA surface through a water-soluble polymer chain, such as pH iindicator hydrophilic HPTS and Fe^{2+} indicator ferrozine (Zhu and Aller, 2012; Zhu et al., 2005). In addition, PVA is also easily available, transparent in the UV–VIS range and hydrophilic properties.

3.2.2. Luminescent indicators

The recently published reviews and books have provided comprehensive introductions and summaries of the performances and characteristics of O_2 luminescent indicators (Bittig et al., 2018; Borisov et al., 2012; Dmitriev and Papkovsky, 2018; Wang and Wolfbeis, 2014), pH luminescent indicators (Han and Burgess, 2009; Wencel et al., 2014) and temperature indicators (Wang et al., 2013). The characteristics, polymer matrix materials, dynamic range of analytes and applications of luminescent indicators and optical microparticles or nanoparticles applied in planar optodes have been summarized in the Tables 3 and 4, respectively. Furthermore, the detail discussions about the performances and characteristics of luminescent indicators were presented in Supporting Information.

3.2.3. Optical insulation layer

An optical insulation layer is coated on top of sensor film. The layer plays an important role in an intensity-based imaging setup, as it can eliminate light scattering from sediments or soils, but also prevent some large particles in sediments or soils from damaging the sensing layer. In some studies, the sensing layer was coated with a thin black silicone to ensure optical insulation (Glud et al., 1996; Klimant and Wolfbeis, 1995); a white, opaque membrane was applied as insulation (Hoefer et al., 2017). In addition, the carbon black, TiO_2, and ZnO_2 nanoparticles were embedded thin translucent silicon/hydrogels as insulation layer (Brodersen et al., 2017; Hoefer et al., 2017; Larsen et al., 2011). For gas-analytes planar optodes (e.g., O_2, CO_2 and H_2S), a gas permeable silicone rubber often be coated onto the top of sensing layer to eliminate the cross-sensitive of various nonvolatile inorganic and organic aqueous ions and molecules.

3.3. Luminescent indicators immobilized methods

Luminescent indicators are generally immobilized into the polymer matrix through physical entrapment or chemical binding. The physical entrapment method as commonly used method is easy and fast, it has been widely applied for preparation of O_2, CO_2, H_2S, pH and

Table 2
Overview of matrix materials, suitable analyte and physicochemical characteristics.

Polymer	Analyte	Characteristics	References
Polystyrene (PS) and its derivatives	O_2	Moderate gas permeability, good optical transparency and mechanical properties, the sensitively and dynamic range of O_2 planar optode are depended on characteristics of PS- derivatives	Koren et al. (2013)
Sol-gel	O_2, pH	Moderate gas permeability, good optical transparent, tolerate high temperatures, not biodegraded, excellent chemical and photochemical stability,	Konig et al. (2005), Koren et al. (2012), Wencel et al. (2009)
Polymethyl methacrylate (PMMA)	O_2, NH_3	Poor oxygen permeability, but useful for high oxygen concentration, good optical transparency, good mechanical properties.	Courbat et al. (2009), Jiang et al. (2017b)
Plasticized- poly (vinyl chloride) (PVC)	O_2, H_2S	Moderate gas permeability, good optical and mechanical properties,	Glud et al. (1996, 1998)
High molecular weight PVC	Temperature	Low oxygen permeability, positive effects on the temperature sensitivity of the indicator	Stich et al. (2008)
Poly(vinyl alcohol) (PVA)	pH, Fe^{2+}, temperature	Low oxygen permeability, easy chemical modification, hydrophilic properties, mechanical flexibility	Peng et al. (2010), Zhu and Aller (2012), Zhu et al. (2005)
Ethyl cellulose (EC)	O_2, H_2S, pCO_2	High gas permeability, good optical transparency and mechanical strength, good photo- and thermal stability	Baleizao et al. (2008), Nagl et al. (2007), Zhu and Aller (2013), Zhu et al. (2006a)
Hydromed D4	pH, extracellular enzyme, NH_3, Temperature, NO_3^-	High gas permeability, water and protons, optically transparent and mechanically robust, equilibrium water contents approaching 50%	Cao et al. (2011), Pedersen et al. (2015a), Rudolph et al. (2017), Stahl et al. (2006), Tobias et al. (2012)
Polyacrylonitrile (PAN)	Temperature	Extremely low gas permeability, low uptake of water, good optically transparent, often used to polymer for optical microparticles or nanoparticles (pH, temperature)	Liebsch et al. (1999), Meier et al. (2011)

temperature planar optodes (Borisov and Klimant, 2008a; Glud et al., 1996; Rudolph et al., 2013; Zhu and Aller, 2013; Zhu et al., 2006a). However, physical entrapment method has several significant shortcomings, which mainly resulted from luminescent indicators can freely migrate in the matrix. Firstly, physical entrapment method is only suitable for immobilize non- or low polar indicators, but not suitable for polar indicators due to the significant leaching problem, such as some polar pH indicators, HPTS and fluorescein isothiocyanate (FITC). Second, simple physical entrapment cannot prevent aggregation between dye molecules with time. Third, diffusion of the dye molecules into adjusting materials such as polymeric support is thermodynamically favored and readily occurs with time (Koren et al., 2012; Zhang and Wang, 1994).

Compared to physical entrapment method, the chemical binding method can prevent the occurrence of leaching and aggregation problems by covalently binding the indicators to the polymer matrix through functional groups, such as the carboxyl group, amine group or sulfonyl group. Furthermore, the covalently grafted methods showed better reversibility and higher photochemical stability than the physically physical entrapment method (Zhang et al., 2011). The pH indicator HPTS and the Fe^{2+} indicator ferrozine have been covalently conjugated on the PVA membrane surface, and both showed great stability (Zhu and Aller, 2012; Zhu et al., 2005). However, these methods are usually more complicated and time-consuming. A powerful approach, named “click chemistry”, has potential to graft the indicator dye onto the polymer (Kolb and Sharpless, 2003; Moses and Moorhouse, 2007). This has been proven to be an effective method to glucose analysis and O_2 imaging in cells (Dmitriev et al., 2014; Odaci et al., 2009). Koren et al. (2012) utilized a dithiol as the nucleophilic substitution of the labile para-fluorine atoms of the pentafluorophenyl residues, then covalent-linking the O_2 indicator onto the click-modified polymer to generate a cross-linked O_2 sensing material. The results showed that the O_2 optode prepared with cross-linked O_2 sensing material had better stability than O_2 optode prepared by physical entrapment method, even exposed within organic solvents. The introduction of click chemistry gives us another reliable choice to improve the stability of planar optodes.

3.4. Luminescent signal enhancement

Luminescent signal enhancement in sensing layer is useful for improving the signal-to-noise ratio, reducing interference from background fluorescence or ambient light. However, increasing the indicator dye concentration to enhance luminescent signal can lead to dye migration and aggregation, and even self-quenching. As such, it is important to identify the most effective methods for increasing sensors brightness. Two main approaches have been developed to enhance the sensors lightness. One is to use light-scattering particles, such as TiO_2, SiO_2, gold silver or diamond, which are entrapped in matrix materials (Chatni et al., 2009; Glud et al., 1996; Gryczynski et al., 2003; Jiang et al., 2017b; Moßhammer et al., 2016). The intensity of light emerging from the sensing layer is increased by particle scattering (Chatni et al., 2009; Precht et al., 2004). In addition, Polerecky et al. (2000) suggested that most of the luminescence emitted by indicators embedded within the very thin sensing layer tend to be trapped within and guided along the supporting layer, if the supporting layer has a higher-refractive index than the ultimate surrounding media (e.g. water, or air). Therefore, the use of light scattering particles like TiO_2 might disturb optical waveguide configuration, leading to much brighter light leaving the optode, and reducing the lateral spatial resolution.

Another method that enhances luminescent sensors brightness is antenna dye. Antenna dye is based on light harvesting, which effectively collects the excitation light energy and transfers the energy to the indicators (Mayr et al., 2009). Antenna dye such as Quantum dots (QDs), Macrolex fluorescence yellow 10GN (MY), as well as Coumarin 6 and Coumarin 545T have been developed to support the imaging of O_2, pH, and NH_3 (Jiang et al., 2017a; Larsen et al., 2011; Mayr et al., 2009). This method of increasing fluorescent sensor brightness is simple, flexible and has only a slight effect on the dynamic range. However, the spectral overlap of antenna dye and indicator dye can make it difficult to separate wavelengths when using a common camera, which could lead to inaccurate measurements. Furthermore, indicators and antenna dyes often require the same excitation bands, which can increase add to the difficulty of choosing the suitable dyes to use in analysis.

3.5. Composite planar optodes

Composite planar optodes have been developed for simultaneous monitoring of multiple parameters at the same or almost the same physical positions by combining multiple luminescent indicators and microparticles or nanoparticles in the sensing layer (Borisov et al., 2011; Ehgartner et al., 2014; Moßhammer et al., 2016; Pedersen et al.,

Table 3
Overview on optical indicators, dynamic range, polymer matrix and applications in planar optodes.

Analytes	Indicator	Polymer matrix	Dynamic	Imaging approaches	Application	References
O_2	PtOEP	PS	0–100% air sat.	PI CR	Microscale water flows; sediments; rhizospheres; seawater	Han et al. (2016), Jiang et al. (2017a), Oguri et al. (2006), Song et al. (2011, 2012)
	PtTFPP	PS Sol-gel	0–100% air sat.	PI RLD CR FD	Sediments, rhizospheres, soils	Christel et al. (2016), Frederiksen and Glud (2006), Koren et al. (2012, 2019), Pischedda et al. (2011)
	Ru-DPP	PS	0– > 100% air sat.	PI FD	Biofilms, sediments, seawater, biofilms,	Glud et al. (1998), Jiang et al. (2017b), Konig et al. (2005), Kuhl et al. (2008),
		Plasticized-PVC Sol-gel PMMA		RLD	biological skeleton	Staal et al. (2011b), Xu et al. (2001)
	Iridium (III) complex	PS	0– > 100% air sat.	PI RLD	Biofilms, benthic microalgal communities,	Borisov and Klimant (2007), Hancke et al. (2014), Staal et al. (2011a)
	$Eu(HPhN)_3dpp$	PS	0–40% air sat.	CR	Microbial mats	Borisov et al. (2014), Moßhammer et al. (2016)
	Fullerene C70	EC Organo-silica	0– > 100% air sat.	RLD	–	Baleizao et al. (2008), Nagl et al. (2007)
pH	Hydrophilic-HPTS	PVA	5.5–8.6	WR	Sediments,	Hakonen et al. (2010), Hulth et al. (2002), Zhu et al. (2005)
	Lipophilic-HPTS	Hydromed D4	6.0–9.0	CR	Sediments	Borisov et al. (2009a), Larsen et al. (2011)
	HPTS-IP	Sol-gel	5.0–8.0	WR	–	Wencel et al. (2009)
	DHFA	Hydromed D4	7.0–9.3	PI t-DLR	Sediments	Schröder et al. (2005, 2007b)
	DHFAE	Hydromed D4	7.0–9.3	WR t-DLR	Sediments	Schröder et al. (2005), Stahl et al. (2006)
	DCIFODA	Hydromed D4	5.5–8	CR	Rhizospheres	Ehgartner et al. (2014), Hoefer et al. (2017)
	aza-BODIPY complexes	Hydromed D4	7.2–8.8	CR	Microbial mats	Ehgartner et al. (2014), Jokic et al. (2012), Moßhammer et al. (2016)
	5-Fluorescein	Hydromed D4	6–8	PI CR	Seawater, rhizospheres	Jiang et al. (2017a, 2018), Rudolph et al. (2013)
H_2S	Pyronin Y	EC	nd-3150 µmol/L LOD: 4 µmol/L	PI	Sediment	Zhu and Aller, 2013
	DPCO-Zn^{2+}	Hydromed D4	0–4000 µmol/L LOD: 4.8 µmol/L	Absorbance	Sediments	Yin et al. (2017)
	TOFMA	PVC	0–735 µmol/L	PI	–	Choi and Hawkins (2003)
*p*CO2	TOA^+PTS^-	EC	0–40 matm LOD: 0.193 matm	WR PI t-DLR	Sediments	Schröder et al. (2007a), Zhu and Aller (2010), Zhu et al. (2006a)
NO_3^-	HPTS-TOA	Hydromed D4	1–50 mmol/L	CR	–	Pedersen et al. (2015a)
Extracellular enzyme	Leu-MCA	Hydromed D4	0.10–0.45 µmol sub/h/g	PI	Sediments	Cao et al. (2011, 2013)
NH_3	Merocyanine 540	Hydrogel and cyano phenyl dodecyl ether	LOD: 2 nmol/L	WR	biological tissues	Strömberg and Hakonen (2011)
	Bromophenol blue	CA Hydromed D4	0–1000 µg/L LOD: 1 µg/L	CR	–	Tobias et al. (2012)
NH_4^+	Merocyanine 540	Hydrogel and cyano phenyl dodecyl ether	10 µM–100 mM	WR	Soils, rhizospheres	Delin and Strömberg (2011), Strömberg (2008), Strömberg and Hulth (2001)
Fe^{2+}	Ferrozine	PVA	nd-200 µmol/L LOD: 4.5 µmol/L	Absorbance	Sediments	Zhu and Aller (2012)
Mn^{2+}	Cd-TSPP	Polyurethane	0–400 µmol/L LOD: 0.3 µmol/L	Absorbance	Sediments	Soto Neira et al. (2013a, 2013b)
Temperature	Eu(III) chelates	PAN	0–50 °C	RLD	–	Borisov and Klimant (2008a)
	$Ru(phen)_3(PF_6)_2$	PAN	0–60 °C	RLD		Liebsch et al. (1999)
	Cr(III)-doped YAB	Hydrogel D4	0–50 °C	RLD		Borisov et al. (2010)

2015b; Schröder et al., 2007a). Typically, different indicators need different wavelength light sources to excite their molecules. The images are recorded at different emission wavelengths with cameras, and several filters are required to reduce the cross-talk between different indicators. In addition, the optical microparticles or nanoparticles incorporated into inert polymer can effectively avoid the fluorescence resonance energy transfer (FRET) between different luminescent indicators (the maximal FRET distance is 10 nm) (Meier et al., 2011). However, the potential risk needs to be considered including leakage of microparticles or nanoparticles and reduction of spatial resolution.

3.6. Composition of PO-DGT

There has been a recent increase in the application of a combined PO-DGT hybrid sensor. The PO-DGT hybrid layer generally consists of support material, a PO sensing layer, DGT binding gel, and protective membrane, the thin DGT binding gel overlying on the surface of PO sensing layer. The preparation of PO-DGT layer mainly consist two method, one is to disperse the DGT adsorbent materials in the hydrogel and then coat it on the surface of the PO sensing layer to obtain a single hybrid sensing layer (Han et al., 2017; Hoefer et al., 2017). Other method is that ultra-thin DGT gel (approximately 50/150 µm thick,

Table 4
Overview on optical micro- and nanoparticles, dynamic range and polymer matrix in planar optodes.

Analytes	Indicator-polymer	Polymer matrix	Dynamic	Imaging approaches	References
O_2	PtTFPP-PS[a]	Hydromed D4	0–100% air sat.	CR	Meier et al. (2011)
	PtTFPP-PSAN[b]	Hydromed D4	0–100% air sat.	t-DLR	Stich et al. (2008)
	PdTFPP-PSAN[c]	Hydromed D4	0–100% air sat.	RLD	Borisov and Wolfbeis (2006)
	$Ir(CS)_2$(acac)-PSAN[d]	EC	–	RLD	Borisov et al. (2011)
pH	FITC-AC[e]	Hydromed D4	4–8	CR	Meier et al. (2011)
	FITC-PAN[f]	Hydromed D4	4–8	t-DLR	Wang et al. (2012)
pCO_2	$HPTS(TOA)_3$-EC[g]	PDMS	–	FD	Borisov et al. (2006)
Temperature	Eu(tta)3(dpbt)-PVC[h]	Hydrogel D4	0–50 °C	RLD	Stich et al. (2008)
	Eu-DT-PMMA[i]	PVA	0–50 °C	RLD	Peng et al. (2010)
	Ru(dpp)-PAN[j]	Hydrogel D4	0–60 °C	RLD	Wang et al. (2012)
	$Eu(tta)_3$L-PAN[k]	Hydrogel D4	0–60 °C	RLD	Borisov and Wolfbeis (2006)

[a] PtTFPP embedded into the polystyrene (PS) polymer.
[b] PtTFPP embedded into the poly(styreneco-acrylonitrile) (PSAN)) polymer.
[c] PdTFPP embedded into the PSAN polymer.
[d] Ir(CS)2(acac) embedded into PSAN polymer.
[e] FITC covalently bound onto the surface of amino-cellulose (AC) particles.
[f] FITC covalently bound onto the surface of amino-functionalized polyacrylonitrile (PAN-NH2) nanoparticles.
[g] $HPTS(TOA)_3$ embedded into ethyl cellulose (EC) polymer.
[h] $Eu(tta)_3$(dpbt) embedded into high molecular weight PVC.B2
[i] Eu-tris(dinaphthoylmethane)-bis(trioctylphosphine oxide) (Eu-DT) embedded into the poly(methyl methacrylate) (PMMA).
[j] Ru(dpp) embedded into PAN polymer.
[k] $Eu(tta)_3$L embedded into PAN polymer.

typical DGT gel is 400/800 μm thick) is mounted onto the planar optode with tape to obtain a double layer sensor (Lehto et al., 2017; Martin et al., 2019). The latter is easier to operate for preparation, but it has potential risk for lateral diffusion of planar optode analytes in the DGT gel.

In addition, studies have found the DGT binding gel can significantly increase the response time (Hoefer et al., 2017; Stahl et al., 2012). This may be attributed to the diffusional barrier caused by overlaying additional DGT gel, and a relatively thick filter membrane. This increase of the diffusion distance of analyte would delay the optical response of the luminophore indicators in the sensing layers. In addition, limited binding capacity of thin DGT gel, dye leakage and transfer, and other artificial factors may affect the sensor performance. Therefore, it remains challenging to develop a sensor capable of DGT and PO measurements.

4. Planar optode imaging system

The imaging system (Fig. 1) mainly consists of an excitation light source and camera. Halogen/xenon arc lamps are equipped with narrow band filters (Glud et al., 1996, 1998; Pischedda et al., 2008) and high-power light emitting diodes (LEDs) typically have narrow band emissions (Hancke et al., 2014; Schröder et al., 2007b). Both of them are used as light sources to excite analyte-sensitive luminescent indicators in planar optode. The lamp disadvantages of high cost and power consumption, the requirement for warming up before use and the difficulty in adjusting excitation light intensity have limited its application (Strömberg et al., 2009a). LEDs have recently become more widely used as an excitation light sources, due to their distinct advantages (i.e. high power-to-size ratio, low cost, narrow emission spectra, stability, and ability to vary light emission in the ~ ns range) (Holst et al., 1998; Strömberg et al., 2009a).

Different imaging methods use different cameras to acquire images. In lifetime-based imaging, a highly light-sensitive fast gateable CCD camera is required to acquire a phosphorescence emission image during intensity decay (μs scale) (Borisov et al., 2011; Holst and Grunwald, 2001; Strömberg and Hakonen, 2011). In intensity-based imaging, both inexpensive DSLR (digital single-lens reflex) and CMOS (complementary metal oxide semiconductor) or CCD camera have been used as detection systems (Lehto et al., 2017; Pedersen et al., 2015a; Song et al., 2012; Zhu et al., 2005). Previous studies using the color ratiometric method have been mostly based on a single-CCD camera, which separates the emission light into three primary colors: red, green, and blue (Jiang et al., 2017a). However, single-CCD camera detects only one-third of the color information for each pixel. The other two-thirds must be interpolated with a demosaicing algorithm to 'fill in the gaps', which results in a much lower effective resolution.

To address this problem, Jiang et al. (2017a) used a 3CCD camera to perform the imaging. Each CCD separately measured the primary colors, red, green, or blue light. This solution can enhance resolution and lower noise; however, this method is limited by the spectral overlap of indicators. Measuring multiple analytes using a composite PO (i.e. two or more indicators immobilized within a single PO membrane) has been applied; however, it is challenging to separate the emissions from the multiple dyes. One simple approach to address this has been to use a 2CCD camera with an RGB camera chip and a NIR camera chip to reduce the cross-talk. The 2CCD set-up allows ratiometric imaging simultaneously in the visible light and in the NIR (Ehgartner et al., 2014; Moßhammer et al., 2016).

4.1. VisiSens system

A robust instrument, called the VisiSens system, has been developed to study analyte distributions and dynamics. Based on the PO principle, the VisiSens system is an integrated system with image acquisition hardware and software to process images (Kumari and Gupta, 2017; Lenzewski et al., 2018; Tschiersch et al., 2011, 2012). VisiSens produces a range of different instruments, designed for various applications. For VisiSens TD system, the fields of view from mm^2 up to 30 cm × 25 cm are possible. In addition, a compact and portable handheld imaging system is suited for laboratory experiments, but can also be used for in situ investigations out in the field. Studies have demonstrated that VisiSens system can be applied to investigate the O_2, pH and CO_2 dynamic in soils, the rhizosphere, stem and leaf of plants, as well as within the developing seed (Faget et al., 2013; Lenzewski et al., 2018; Tschiersch et al., 2011, 2012), and O_2 dynamics in the oak wood of wine barrels (Nevares et al., 2014). The VisiSens system can be highly beneficial for other research areas, such as biotechnology or medicine. VisiSens system is the first commercially available from PreSens GmbH, Regensburg, Germany.

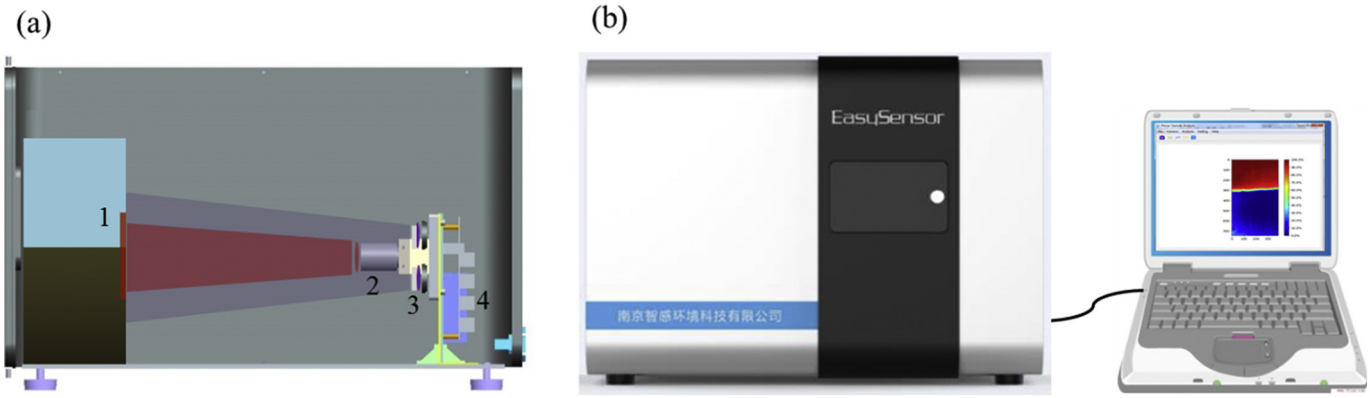

Fig. 3. (a): the section structure of planar optode analysis equipment consisting of 1 planar optode, 2 the CCD camera system (including camera, lens and filter), 3 the excitation source system (including LEDs, filters and diffusers), 4 the power source and trigger; (b): the appearance structure of planar optode analysis equipment (www.easysensor.net).

4.2. Planar optode analysis equipment for laboratory imaging

Recently, Nanjing EasySensor Environmental Technology Co., Ltd. developed a novel planar optode analysis equipment for O_2, pH and pCO_2 imaging in laboratory (www.easysensor.net). As shown in Fig. 3, this PO analysis equipment consists of the sealed box and computer control system. In the sealed box, the four different excitation light sources include 415 nm LEDs for O_2 and pCO_2 measurements; 425 nm LEDs for pH measurement; 470 nm LEDs for pCO_2 measurement; 505 nm LEDs for pH measurement, and every LED equips with diffusers for obtaining uniform excitation light. Additional 485 nm and 515 nm short-pass filters are equipped in the front of 470 nm and 505 nm LEDs to eliminate interferences of impure excitation lights, respectively. Three different band-pass filters as emission filters are equipped in the front of the CCD camera (515 nm, 545 nm, and 650 nm for pCO_2, pH, and O_2 measurements, respectively). In addition, the self-developed printed circuit board is used to modulate the LEDs and image capture. The sealed box provides the dark environment, which can minimize external light interference. Furthermore, this analysis equipment with moderate volume (650 mm (length) × 450 mm (width) × 450 mm (height)) is suitable for laboratory simulation experiments of sediments and soils.

4.3. In situ measurement devices of planar optodes

PO has been widely applied for imaging studies in laboratory microcosms to acquire 2D distributions and dynamics of analytes. However, there have been few field applications of PO, largely because of the complex experimental setups and devices (Vieweg et al., 2013). In situ deployment was first performed by Glud et al. (2001) to obtain 2D O_2 distribution in benthic sediments in shallow water. In filed studies, the central instrument housing is mounted on an inverted periscope and contains, the excitation light source, optical filters, CCD camera and associated electronics. The CCD camera is connected to a personal computer (PC) at the surface using a fiber optical link (Fig. 4a, b). The instrument is a powerful tool for field applications and has been applied to study the effect of fauna activity and photosynthesis on O_2 distribution (Wenzhöfer and Glud, 2004).

Another in situ sediment profile imaging (SPI) instrument, CHEM-SPI, has also been used in filed studies (Fig. 4c, d) (Fan et al., 2011). This CHEM-SPI system loaded three adjacent fluorosensor foils, which simultaneously measured vertical sections of pH, O_2, and pCO_2 distributions, and recorded visible images of the sediment structure closely associated with the solute fluorescence images. Later, the optical system and electronics of CHEM-SPI were simplified, leading to the development of the CHEM-SPII-2 benthic sensing system. The CHEM-SPII-2 imaging system has been used in situ to measure 2D dissolved Mn^{2+} and Fe^{2+} in marine sediments (Soto Neira et al., 2013a, 2013b). This technique has been applied in sediment environments; however, relatively large PO devices can disturb the natural sediment structure. Moreover, field applications of PO are only suitable in fine-grained marine and shallow lacustrine settings, which allow the instrument to be easily inserted into the sediment. It is difficult to apply the tool in coarser, sandy to gravelly sediments (Glud et al., 2001; Vieweg et al., 2013).

5. Application of planar optodes

5.1. Application of O_2 optodes

5.1.1. Sediments

As a high resolution, in situ measurement technique, PO has been widely focused on O_2 distributions and dynamics in sediments. The spatial and temporal 2D O_2 concentration gradient at the SWI was first observed using planar optode (Glud et al., 1996); other researchers have observed similar results (Glud et al., 2001; Oguri et al., 2006). Moreover, O_2 optodes are suitable for investigating O_2 dynamic changes in sediments due to their long-term stability and rapid response time. For example, Behrens et al. (2007) evaluated the distribution and dynamic of O_2 around buried sandeels (*Ammodytes tobianus*) in sediment. *Ammodytes tobianus* can live in anaerobic sediments using inverted porewater cones, allowing these organisms to obtain oxygen from the overlying waters. Similarly, Wenzhöfer and Glud (2004) investigated the effects of fauna activity for O_2 distributions and dynamics in sediments, using the in-situ instrument containing planar optodes. Through this technique, they characterized the spatial and temporal variability of O_2 (timescale: days) and found that fauna activity can stimulate changes in O_2 dynamics, which could affect benthic mineralization (Glud et al., 2016; Pischedda et al., 2010). However, these studies give snapshots of O_2 dynamic at different stages but do not manage to capture the true dynamic changes of oxygen concentrations in the sediments.

The true O_2 dynamics in sediments were captured in various condition, e.g. ripple movement (Precht et al., 2004), organic matter degradation (Franke et al., 2006) or affected by bioirrigation (Murphy and Reidenbach, 2016; Pischedda et al., 2011; Polerecky et al., 2006; Volkenborn et al., 2010, 2012). The waves could significantly increase the O_2 penetration, which changed from depths of ~ 3 mm to depths ~ 5 mm in sediment surface. The oxygen consumption rates at locations of the particular organic matter sediments can reach to 18-times higher than the surrounding sediments. In addition, burrowing macrofauna and bioirrigation as sediment conduits can cause overlying oxygenated water to penetrate the sediment, increasing the heterogeneity of oxygen distribution, and influencing biogeochemical processes of other

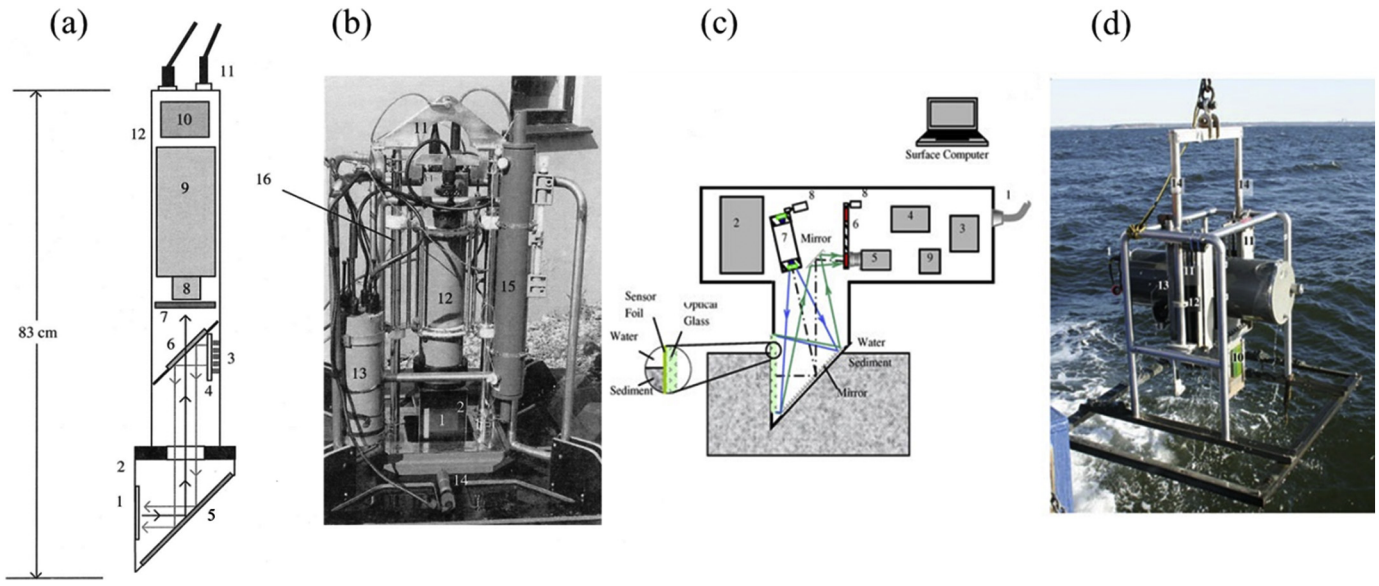

Fig. 4. (a) and (b) Illustration of the central housing and the periscope head and in situ measurement device, respectively: 1 PO, 2 sensor window, 3 LEDs, 4 diffuser, 5 mirror, 6 dichroic mirror, 7 excitation filter, 8 lens, 9 CCD camera, 10 electronics controlling the excitation light, 11 connectors (one optic and one electric), 12 central housing, 13 battery for video and light, 14 video camera, 15 niskin bottle, and 16 positioning elevator (Glud et al., 2001). Reprinted with permission from Glud et al., Copyright (2001), John Wiley and Sons; (c) and (d) schematic cross-section of multispectral imaging system and in situ measurement device, respectively: 1 Umbilical cable, 2 constant current power module for LEDs, 3 power supply for steppers, 4 stepper driver, 5 digital camera, 6 emission filter wheel, 7 LED wheel with excitation filters, 8 steppers, 9 power supply for camera, 10 optical window with PO attached, 11 lead racks, 12 adjustable collar, 13 hydraulic cylinder with flow control valve, 14 lifting arms (Fan et al., 2011). Reprinted with permission from Fan et al., Copyright (2011), Springer Nature.

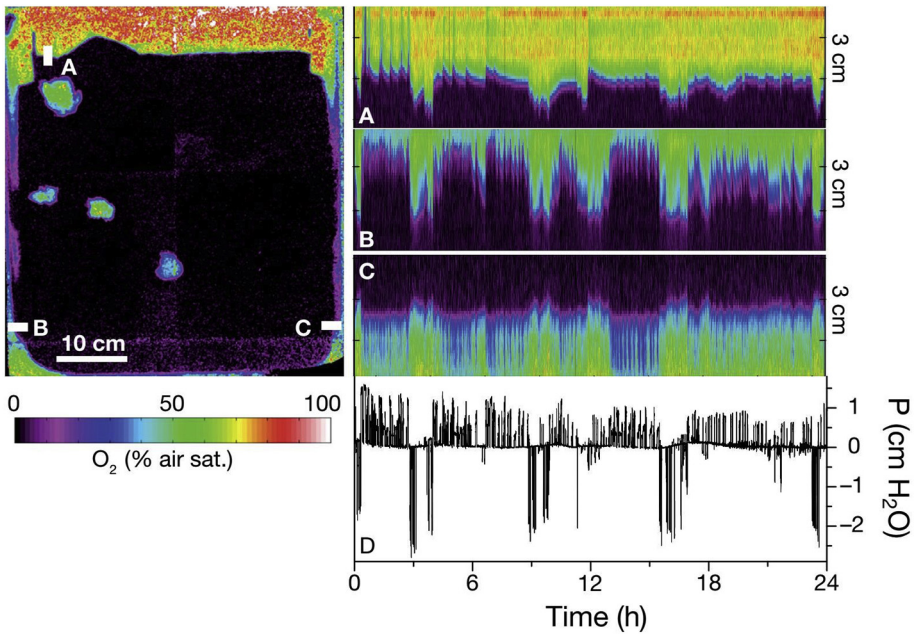

Fig. 5. A, B and C demonstrate the dynamics of O_2 within 24 h of analysis, along 3 cm profiles in sediment-water interfaces. D is the corresponding synchronous porewater pressure at the sediment-water interface (Volkenborn et al., 2012). Reprinted with permission from Volkenborn et al., Copyright (2012), Inter-Research.

elements (Fig. 5). The oxygen consumption rates in different sediment depths can be easily measured, based on continuous O_2 concentration profiles obtained by PO with high temporal-spatial resolution (Polerecky et al., 2005; Precht et al., 2004). Moreover, these were probably the first studies where the dynamic component information captured by PO was actually quantified and interpreted in the context of sediment biogeochemistry.

The recent combination of PO and DGT techniques has been applied a combined PO-DGT sensor to simultaneously measure dissolved O_2 and trace metal dynamics in sediment (Lehto et al., 2017; Stahl et al., 2012). The exchange of overlying oxygenated water drives a gradual increase in the O_2 concentration around the burrows; this exchange then affects metal mobilization in irrigated burrows (Stahl et al., 2012). Organic matter deposition can induce highly localized anoxic conditions or high oxygen consumption rates at the SWI (Franke et al., 2006), increased Fe and Mn mobilization, and the S(II) increase reduced Co, Ni and Zn due to the co-precipitation (Lehto et al., 2017). These studies enhance our understanding of biogeochemical cycle processes induced by redox condition at the SWI.

5.1.2. Biofilms

Planar optode is also an ideal tool for studying O_2 dynamics in biofilm, living cells, biological tissues, and microbial activity due to its high spatial resolution, rapid response, and high sensitivity (Borer et al., 2018; Kuhl et al., 2007, 2008; Xu et al., 2001). For example, Glud et al. (1998) suggested that average O_2 saturation decreased and the heterogeneity increased at the base of biofilm, as the biofilm developed. The heterogeneity of O_2 distribution depended on high biomass clusters and the free flow speed of the overlaying water lying above the biofilm. The study of Kuhl et al. (2007) showed that the O_2 spatial distribution at the biofilm became significantly more heterogeneous with the increased flow. Furthermore, the relationship between biomass and O_2 distributions was developed under both steady state and non-steady state conditions. This demonstrated that O_2 distributions in biofilms change dynamically in response to flow and substrate conditions (Staal et al., 2011a, 2011b). Prest et al. (2012) performed biofilm activity measurements in operating membrane systems using O_2 optodes. They clearly identified low and high activity areas based on O_2 concentration distribution imaging.

5.1.3. Soils

Planar O_2 optodes have also been used to study the effects of O_2 availability on greenhouse gas emissions, such as CO_2, N_2O and CH_4 in soils or fertilized soils (Askaer et al., 2010; Christel et al., 2016; Elberling et al., 2011; Van Nguyen et al., 2017; Zhu et al., 2014). Some studies have found that small-scale soil heterogeneity strongly affects the spatial distribution of O_2 availability in wetland soils. O_2 controls the CH_4 oxidation under aerobic conditions, and CH_4 can be produced in anoxic zones (Askaer et al., 2010). The availability and spatial distribution of O_2 in soil are controlling factors in N_2O production and emissions to the atmosphere. After manure was added to the soil, an anoxic layer formed rapidly around the layered manure. Uniformly distributed manure led to a more widespread anoxia, and the emission rates of N_2O increased immediately with O_2 depletion (Zhu et al., 2014). Other studies have found similar results (Van Nguyen et al., 2017). In addition, research found that manure degradation resulted in increased O_2 consumption, and more CO_2 was released from the manure solid-amended soil (Christel et al., 2016).

5.1.4. Rhizospheres

Frederiksen and Glud (2006) investigated the radial oxygen loss (ROL) processes in rhizosphere of *Zostera marina* using planar optode. Studies showed the of rhizosphere is not only driven by the day/night lighting cycle, but also by the oxygen content of the water. Furthermore, the ROL of rhizosphere was localized to the root apical, extending up to 8 mm along the root. Other studies have found similar results around the plant rhizosphere in soils or sediments (Jovanovic et al., 2015; Koop-Jakobsen and Wenzhöfer, 2014; Koren et al., 2015). Larsen et al. (2015) used a planar O_2 optode to investigate O_2 dynamics in the rhizosphere of young rice plants. The study revealed that different parts of the rhizosphere exhibited a high spatiotemporal heterogeneity in rhizosphere O_2 dynamics and differences in the radial oxygen loss. In addition, the heterogeneously distributed metal plaques along the root were observed, which were corresponding with the oxic zone adjacent the root. The form of metal plaques in rhizosphere is critical for plant uptake of nutrients (Wei et al., 2019; Xing et al., 2018). Marzocchi et al. (2019) further investigated O_2 dynamics in the rhizosphere of *Vallisneria spiralis* and its implication for nutrient availability combining PO and microplate sampler. The depletions of both NH_4^+ and PO_4^{3-} in the rhizosphere were observed, resulted from ROL of rhizosphere and plant uptake process.

Recently, several studies have combined O_2 optodes with microbial community profiling to investigated the relationships between ROL and the abundance, activity, and spatial orientation of cable bacteria (Martin et al., 2019; Scholz et al., 2019). The cable bacteria is ubiquitous and actives in the rhizosphere of aquatic plants whether in seawater or freshwater, furthermore, the higher densities and activities of cable bacteria around the rhizosphere than the bulk sediments. Therefore, the ROL and it induced the abundant cable bacteria in the rhizosphere can protect the root from toxic, free sulfide (Brodersen et al., 2018; Jensen et al., 2007). The combination of O_2 optode, DGT and microbial community profiling provide an effective tool to rethink sediment biogeochemistry after the discovery of cable bacteria.

Furthermore, Williams et al. (2014) used PO-DGT sandwich sensors to interpret the effect of ROL and pH on the mobility of heavy metals in roots in wetland soil. The root-induced O_2 enrichment and pH decrease increased the mobilization As, Pb, and Fe(II) adjacent to the root tips compared with bulk soil, especially, the Fe(II) flux at the root tips was 3- and 27-fold higher than the anaerobic soil and aerobic rooting zone, respectively. Brodersen et al. (2017) combined PO with DGT to study seagrass-mediated phosphorus and iron solubilization in tropical sediments. The seagrass-mediated the reduction of ~0.8 pH at the basal leaf meristem of rhizosphere, which resulted in the ~20 and 10-fold concentration increase of phosphorus and Fe(II), respectively. The results showed that phosphate was released to meet the nutritional needs of seagrass through the ROL and local acidification of the rhizosphere, which results in dissolution of carbonates and organic carbon, reduction of insoluble Fe(III) oxyhydroxides and sulfide oxidation to release P.

O_2 is one of the most important biogeochemical factors that can affect cycling of various important elements, e.g. carbon, nitrogen, phosphorus, sulfur and metals (Glud, 2008). Planar O_2 optodes can simultaneously map the 2D media structures (e.g., burrows, biofilms, and rhizospheres) and O_2 dynamics with a spatio-temporal resolution of sub-mm and a few seconds. The combination of O_2 optodes and other analysis technologies will bring us more critical information to understand the biogeochemical processes. However, the O_2 optodes is particularly sensitive to temperature, especially during the in-situ measurement in marine or lake. Therefore, in order to ensure the precise and reliable measurements, the compensation or calibration for the temperature effects need to done.

5.2. Application of pH optodes

5.2.1. Sediments

Significant pH gradients have been found between the overlying water and sediment, and adjacent to burrow structures (Hakonen et al., 2010; Hulth et al., 2002; Zhu et al., 2005, 2006b). The pH distributions and dynamics in the sediments can be changed by the presence of burrows that are induced by the pumping of overlying water into sediments. The completely infilled structures become low pH sites ($>$ 1 pH unit lower than the overlying water), due to the degradation of locally elevated reactive substrates (Zhu et al., 2005, 2006b). Additionally, the in-situ seasonal measurements indicated the pH in sediment is depended on temperature, organic matter inputs, and macrofaunal activities, which play a vital role for diagenetic process (Fan et al., 2011).

5.2.2. Rhizospheres

The pH distributions and dynamics in the rhizosphere have strongly relationship with plant species and soil type (Blossfeld et al., 2010; Sun et al., 2019). *alpine pennycress* and *ryegrass* alkalinized rhizospheres by up to 1.7 and 1.5 pH units, respectively, whereas *maize* acidified its rhizosphere by up to approximately 0.7 pH units. Other studies have also shown that roots can drive the pH change of surrounding roots in sediments and soils, and pH varies as a function of the distance from root surface, location along root axes, and root maturity (Faget et al., 2013; Kreuzeder et al., 2018; Rudolph et al., 2013). Rudolph et al. (2017) used a device with a glass rhizotron equipped with pH and O_2 sensitive sensor foils. This allowed the mapping of water content, oxygen, and pH dynamics in the rhizosphere of young maize roots, which indicated the pH and O_2 distributions are depended on the

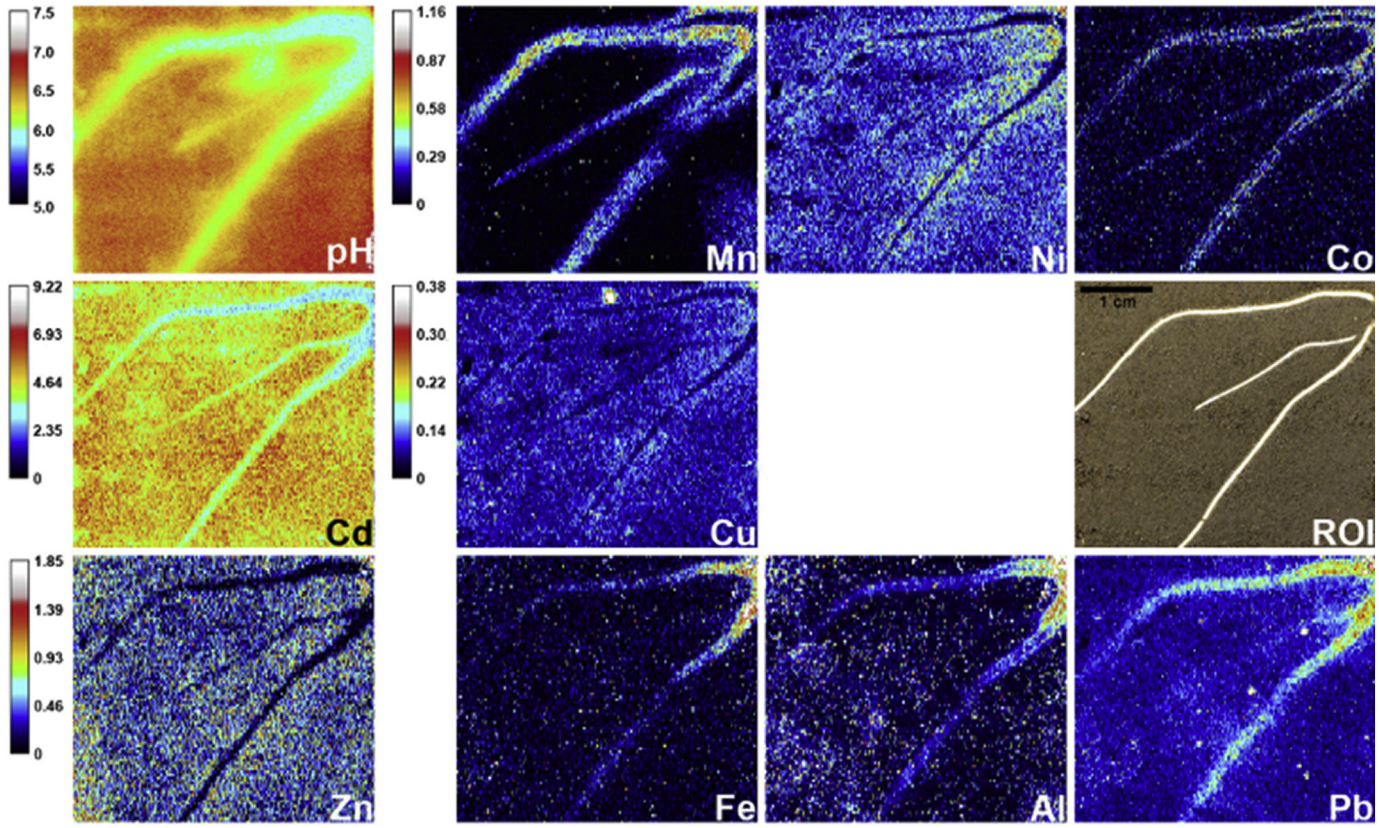

Fig. 6. Images of pH were recorded 23 h after gel application; PO and DGT images show the trace metals average flux to the gel during the exposure period in a *Salix smithiana* rhizosphere (Hoefer et al., 2017). Reprinted with permission from Hoefer et al., Copyright (2017), Elsevier.

rhizosphere age and water content around the rhizosphere.

Furthermore, the relationships of pH distribution and metal available in the *Salix smithiana* rhizosphere were investigated using a hybrid PO-DGT sensor (Hoefer et al., 2017). The rhizosphere induced acidification in root soil was accompanied by the increase metal flux of Al, Co, Cu, Fe, Mn, Ni and Pb, indicating pH-induced metal solubilization around the rhizosphere (Fig. 6). The results of this study are slightly different from that of Williams et al. (2014), which caused by different soil properties and plant species.

5.2.3. Other fields

Some hybrid planar optode sensors have been introduced to simultaneously measure the pH and O_2 in seawater, and microbial mats (Jiang et al., 2017a; Moßhammer et al., 2016). Jiang et al. (2017a) used a composite sensor to reveal the effect of rain drops on pH and O_2 distributions and dynamics in the surface water. Within 40 s after rainfall, the O_2 content increased 2.3 mg/L and the pH value decreased to 7.2. The simultaneous imaging of pH and O_2 revealed dynamic changes as a function of irradiance in a microbial mat, the pH and O_2 concentration increased with mat photosynthesis (Moßhammer et al., 2016).

The pH value is another key parameter that can reflect multiple biogeochemical reactions and transport processes, e.g., C, N, S cycling, metal availability (Gambrell et al., 1991), soil fertility (Buss et al., 2018). The complex distributions and dynamics of pH in microenvironments (e.g., borrows, rhizosphere) have been quantified and visualized using pH optodes. The major limitation of common pH optode based on the hydrophilic-HPTS is that it is sensitive to ionic strength. Other lipophilic luminescent indicators such as 5-Fluorescein, 6,8-dihydroxypyrene-1,3-disulfonic acid (DHPDS) and 20,70-dihexyl-5(6)-N-octadecyl-carboxamidofluorescein (DHFA) have negligible responses to ionic strength. However, these pH optodes are often of high cost or poor stability. In addition, theses current planar pH optodes can be achieved only for a narrow range of pH, with the dynamic range usually limited to approximately $pK_a \pm 1$ or 1.5. The work range of pH optodes should be further broadened to be applied in some environments where the pH varies greatly.

5.3. Application of pCO_2 optodes

5.3.1. Sediments

CO_2 dynamics at the microscale significantly support an understanding of carbon cycling processes. Research using a pCO_2 optode revealed a steep pCO_2 concentration gradient between the overlying water to sediment, and a thin diffusive boundary layer is evident at the SWI (Zhu et al., 2006a). In addition, planar pCO_2 optode was also used to study CO_2 distributions and dynamics in bioturbated sediments (Zhu and Aller, 2010; Zhu et al., 2006a). The results showed a relative decrease in pCO_2 in the inhabited well irrigated burrows compared to surrounding sediment, in contrast, those abandoned burrows have higher pCO_2. The increased pCO_2 around the abandoned burrows were resulted from elevated respiration and a residual influence of burrow formation on microbial activity.

5.3.2. Rhizospheres

The CO_2 dynamics in rhizosphere of *Viminaria juncea* have been obtained using the pCO_2 optode (Blossfeld et al., 2013). According to the pCO_2 dynamics imaging within 3 days, pCO_2 distributions within the entire root rhizosphere, and pCO_2 significantly increased as a function of root growth. Lenzewski et al. (2018) investigated the dynamics of CO_2 and O_2 in the rhizosphere of *Lobelia dortmanna* in different light conditions. In light conditions, researchers observed that there was an aerobic zone with a radius of 3 mm, a CO_2-depleted zone with a radius 2 mm at the root surface (due to root-mediated CO_2

uptake), and a CO_2-rich zone with a radius 10 mm around the root (due to microbial CO_2 production). However, in light-limited conditions, root-mediated CO_2 uptake was stopped and the CO_2-depleted zone eventually disappeared. Results indicated that photosynthetic O_2 production could elevate O_2 release in the rhizosphere, and that increased O_2 concentrations could stimulate the microbial community in sediment, increasing the supply of inorganic carbon for photosynthesis by building up a CO_2 reservoir around the root.

pCO_2 optodes have presented new insights into the cycling and transport of carbon in sediments and rhizosphere. Nevertheless, the pCO_2 optodes easily suffer from the interference of temperature and H_2S (Zhu and Aller, 2010). Especially in marine sediments, high H_2S concentration can severely interfere with CO_2 measurements. Therefore, the measurement using pCO_2 optodes can be done in low H_2S concentration ($< 100\,\mu M$) and stable temperature conditions, or making compensation in combination with temperature sensor.

5.4. Application of NH_4^+ optodes

PO methods have been used to investigated ammonium concentrations, diffusion, and transport in soil after fertilization (Strömberg and Hulth, 2005). The release and mobilization of ammonium in pore water was studied following the dissolution of a fertilizer stick in soil. Results revealed sharp concentration gradients (200×10^{-6}–4500×10^{-6} M) over distances of < 10 mm close to the fertilizer stick (Strömberg and Hulth, 2006). Another study compared ammonium responses after the fertilization of sandy loam and clay with different manures (Strömberg et al., 2009a). Different soil types resulted in a significant difference in ammonium concentrations as a function of time. Spatial movements of ammonium were generally limited in clay than in sandy loam. Other studies have found that when manure is applied at different locations in the soil, the ammonium diffuses differently. For example, the ammonium was distributed across a larger soil volume when manure was applied below the soil surface, rather than above (Delin and Strömberg, 2011).

The main limitation of NH_4^+ optode based on the solvent sensitive dye MC 540, is that it is susceptible to interferences of ionic strength and potassium ions (K^+). The high ionic strength can induce the aggregation of MC 540, causing the formation of less fluorescent or non-fluorescent forms. The K^+ has a possible competitive selectivity for NH_4^+ measurement, due to the comparable binding characteristics to the crown ether nonactin.

5.5. Application of H_2S optodes

Zhu and Aller (2013) developed a novel H_2S optode to study the spatial and temporal 2D H_2S distributions in bioturbated salt marsh sediment. The application of 2D imaging revealed that H_2S concentrations in the burrow wall were low or close to zero. The images clearly revealed a sub-boundary around the burrows, due to the injection of overlying oxygenated water (Fig. 7). Some transient phenomena were also documented. For example, abandoned and refilled burrows and the mucus trails left by macrofauna, such as the polychaete *Nepthys incise*, became hotspots of microbial decomposition activity for approximately 1–2 days following formation (Fig. 7). This activity was associated with elevated H_2S levels. This H_2S optode was not completely reversible in high H_2S concentrations. In addition, the measurements of H_2S optode were limited within 5–6 measurement cycles in high H_2S concentrations. Otherwise, relatively high measurement error could be introduced due to the losing response. An irreversible H_2S planar optical sensor was applied in the bioirrigated sediments, based on the absorbance (Yin et al., 2017). The similar distribution trends of H_2S in marine sediment were observed with Zhu and Aller (2013).

5.6. Application of Fe^{2+} optodes

Planar optodes have been widely used to study O_2, pH, and pCO_2; however, few studies have examined metal distributions. Zhu and Aller (2012) developed an irreversible planar optical sensor to determine the 2D distribution of Fe^{2+} in marine sediments, based on absorbance. The results showed that complex heterogeneous distribution patterns of Fe^{2+} were related to the physical structure and other natural diagenetic heterogeneity. Low Fe^{2+} concentration ($< 5\,\mu M$) cannot be detected in the oxic zone of the sediment, due to rapid Fe^{2+} oxidation. The single use planar optical sensor has also been used to collect in situ 2D distributions of Fe^{2+} and Mn^{2+} in marine surface (Soto Neira et al., 2013a, 2013b).

Fe^{2+} optode is an irreversible sensor, which cannot be used for the study of reaction dynamics. Compared with other planar optodes (e.g. O_2 and pH), it requires relatively long equilibration time (10–30 min). However, compared with other reversible Fe^{2+} imaging approaches based the DET (Cesbron et al., 2014; Robertson et al., 2009; Thibault de Chanvalon et al., 2017), the Fe^{2+} optode shows faster response, and has better stability, easier imaging steps and a lower cost. In addition, the Fe^{2+} is boned by Ferrozine to form Ferrozine-Fe^{2+} complex in the surface of sensor membrane and the Fe^{2+} optode is approximately 10 μm thick, which can effective eliminate the lateral diffusion of Fe^{2+} in the membrane and provide more stable reaction.

6. Outlook and conclusions

6.1. The wall effect

The wall effect cannot be avoided when using planar optodes, whether application involves simulating sediment or soil environments in the laboratory or in situ measurement in the field. The presence of a planar optode (physical boundary) in the middle of a 3D section of sediments/soils can affect the gradients and dynamics of dissolved analytes. In fact, half of the biogeochemical activities in sediments or soils are absent when the planar optode is inserted. Polerecky et al. (2006) carried out a comprehensive evaluation for the wall effect when planar optode was applied in bioirrigated sediments. They found: (1) if the burrows are adjacent to O_2 optode, the oxygen consumption capacity of the sediment around burrows is lower, especially in the areas of the planar optode side of the burrow. The missing oxygen consumption capacity cannot be immediately compensated, leading to an overestimation of the effects of bioirrigation on oxygen exchange at the sediment-water interface. (2) if the burrow is too far away from the O_2 planar optode, O_2 can be consumed before it reaches the planar optode, leading to an underestimation of the effects of bioirrigation. This is also true when using planar optodes in rhizosphere studies in sediments and soils. Consequently, more effective models and methods are still required to obtain a reasonable interpretation of the dynamics and gradients of analytes based on measurements taken using planar optodes.

6.2. Micro- and nanoparticles based sensors

The micro- and nanoparticles based sensors have been proven to be an effective approach to overcome the wall effect (Moßhammer et al., 2019). Optical micro- and nanoparticles are prepared by entrapping the luminescent indicators into nanobeads or polymers. Several simple and effective methods are applied to produce optical micro- and nanoparticles, such as precipitation (Borisov et al., 2009a, 2009b), polymer staining (Borisov and Klimant, 2008b) and mini-emulsion solvent evaporation (Mistlberger et al., 2010). Micro- and nanoparticles can be coated on sample surfaces or embedded into samples, allowing for visualization and quantification of chemical gradients over 2D and 3D structures. Koren et al. (2015) investigated the O_2 distribution and dynamics in the whole seagrass rhizosphere under light and darkness conditions by embedding optical O_2 nanoparticles into a transparent

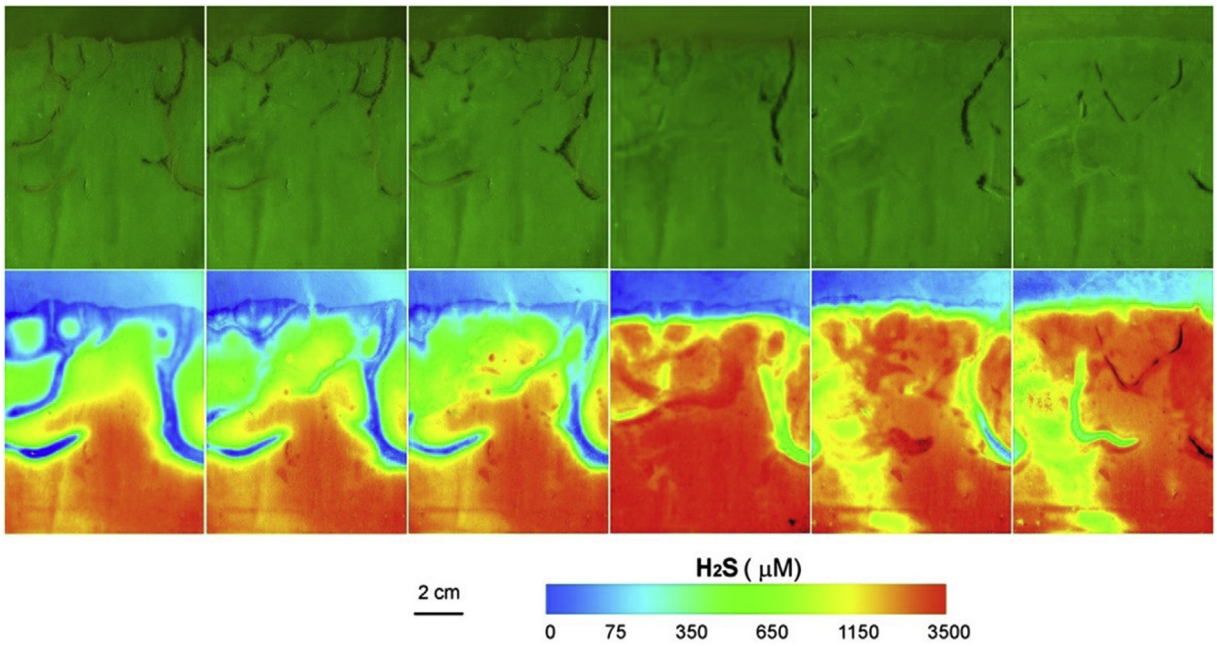

Fig. 7. the change of the structure of bioturbated sediment and the corresponding H_2S distribution with time (Zhu and Aller, 2013) Reprinted with permission from Zhu and Aller., Copyright (2013), Elsevier.

artificial sediment matrix. Furthermore, Elgetti Brodersen et al. (2016) further mapped spatio-temporal dynamics of pH and O_2 of the whole seagrass rhizosphere under different temperature and light conditions. In addition, the micro- and nanoparticles based sensors are also used to visualize O_2 distributions and dynamics on various complex surfaces, including sediment-water interface (Murniati et al., 2016) and coral surfaces (Koren et al., 2016), or within transparent organisms (Glud et al., 2015). The micro- and nanoparticles based sensors can reduce or eliminate the wall effect, while providing fast response and high accessibility for analytes due to the high surface to volume ratio of the optical micro- and nanoparticles (Moßhammer et al., 2019). Currently, only O_2 and pH micro- and nanoparticles based sensors were applied for the studies of biogeochemical progresses, while the other micro- and nanoparticles based sensors such as pCO_2, H_2S and NH_3, have tremendous development and application potential.

6.3. Multi-analyte imaging

The multi-analyte planar optides do not truly measure the multiple analytes at the same spatial-temporal point, because some analytes have to diffuse a few extra micrometers to reach the respective sensing layers (Pedersen et al., 2015b). Despite this fact, hybrid planar optodes have the potential to provide real-time imaging of multiple analytes simultaneously using multiple indicators incorporated into a single sensor. However, to data, this technique has been limited to monitoring only two or three physic-chemical parameters simultaneously.

The development of spectroscopic imaging, called hyper-spectral imaging approach, has the potential to overcome the long-standing problem of cross-talk between absorbance spectrums. The hyper-spectral imaging measures the complete spectra rather than just light intensity integrated over narrow bands, thus allowing differentiation of the different sensor response by spectral decomposition (Polerecky et al., 2009b). Hyper-spectral imaging has been successfully applied in the analysis of pigments in mixed microbial communities and monitoring of the temporal dynamics of plant leaf water content (Ge et al., 2016; Polerecky et al., 2009a). In addition, this technique (combined with DET) has been used in the simultaneous 2D imaging of Fe^{2+} and P, as well as NO_2^- and NO_3^- in sediments (Cesbron et al., 2014; Metzger et al., 2016). Thus, the hyper-spectral imaging is a good prospect for further development and use in multiple analyte imaging using planar optodes.

6.4. Expanding the measurement capabilities of planar optodes

PO has been mainly applied to measure O_2, pH, pCO_2, H_2S, Fe^{2+}, Mn^{2+}, temperature and ammonium; few studies have measured other anions and redox metals. These aspects need further research attention, such as metal cations, oxyanions and enzyme activities. Combining PO and other measurement technologies (especially DGT) is other effective approach for broadening the range of analytes. PO-DGT has been developed to simultaneously 2D image O_2 and labile P/trace metal dynamics, as well as pH and trace metal dynamics. The combination of pCO_2, temperature and NH_4^+ PO analytes with trace metal and other elements associated with DGT analytes need to further exploited. Optimizing the trade-off between DGT capacity and PO response time, as well as the portability and capacity for multi-parameter measurements, are critical for the advance of PO-DGT technique.

6.5. Improvement the environmental monitoring capabilities of planar optodes

The rapid response time and long-term stability of planar optodes make them suitable for use in in-situ monitoring of analyte dynamics in sediments and soils. However, most researchers still use laboratory and mesocosm studies to obtain the spatial and temporal distribution and dynamics of analytes in sediments/soils. Only a few studies have used planar optodes for field measurements in marine sediments, as the in-situ equipment is a relatively large with a complex experimental setup (Fan et al., 2011; Glud et al., 2001; Wenzhöfer and Glud, 2004). Rickelt et al. (2013) developed a novel in-situ O_2 measurement device equipped with 10 vertical O_2 sensors. Each O_2 sensors were made by fixing the O_2-sensitive indicator on surface of polymethyl methacrylate plastic fiber material. This in-situ O_2 sensor was able to track analyte dynamic for 3 consecutive weeks in a peat soil environment. Furthermore, studies suggested that six of the ten sensors could still have stable performance after 4 years of deployment (Rickelt et al., 2013). In addition, Vieweg et al. (2013) also constructed a novel in-situ O_2 measurement instrument and successfully obtained the O_2 dynamic in the

sediment. This sensor was constructed with an O_2-sensitive layer mounted on the outside of the acrylic tube, and quantified O_2 concentration along the sediment profile using a piston equipped with excitation and detection systems, inside the acrylic tube. These studies have proved that the planar optode has great potential for use in in-situ and real-time monitoring. Furthermore, the technology can be expanded to other analytes, such as pH, pCO_2, NH_3 and H_2S. Therefore, application of planar optodes in real-time monitoring and evaluation of the dynamics of various analytes in sediments or soils represents an important way forward in the fields of biogeochemical process studies and environmental risk assessment.

6.6. Future developments in applied fields

A large amount of applied research has demonstrated the effectiveness of planar optodes for the study of biogeochemical processes within sediments and soils. In addition, their non-invasive, real-time, high resolution and user-friendly characteristics make planar optodes suitable for investigating pathogenesis of various diseases. In vivo oxygen-detection systems (based on the planar optode imaging principle) are well established for monitoring the O_2 dynamics in mouse skin tissue (Hofmann et al., 2013; Warnat et al., 2012), embryos (Zhu et al., 2015) and free parascapular flap in the patients (Gehmert et al., 2011). Monitoring of O_2 dynamics in skin tissue is important, as it can help us gain a better understanding of tissue oxygenation and pathogenic pathways of various associated diseases. Therefore, in addition to research on the biogeochemistry in sediments or soils, planar optodes should be pursued in further in vivo research concerning the metabolism and physiology of humans and test animals.

7. Conclusions

This review provides a detailed discussion on the principles, composition, characteristics, and applications of POs, noting their obstacles to move forward and some effective solutions. Planar optodes have broad spaces for development in the biogeochemistry, especially for use in sediment and soil analysis and in combination with other sampling techniques and advance modeling. Therefore, more attention needs be given to promote the advancement of this technology.

Acknowledgments

This research work was financially supported by the National Natural Science Foundation of China (41621002, 41701570, 41877492 and 41701568), the Natural Science Foundation of Shandong Province (ZR2016DM10), CAS Interdisciplinary Innovation Team, and Research instrument and equipment, and Development Project of the Chinese Academy of Sciences (YJKYYQ20170016), National key Research and Development plan (2018YFA0903000).

Appendix A. Supplementary data

Supplementary data to this article can be found online at https://doi.org/10.1016/j.earscirev.2019.102916.

References

Askaer, L., Elberling, B., Glud, R.N., Kühl, M., Lauritsen, F.R., Joensen, H.P., 2010. Soil heterogeneity effects on O_2 distribution and CH_4 emissions from wetlands: in situ and mesocosm studies with planar O_2 optodes and membrane inlet mass spectrometry. Soil Biol. Biochem. 42 (12), 2254–2265.

Bachar, A., Polerecky, L., Fischer, J.P., Vamvakopoulos, K., de Beer, D., Jonkers, H.M., 2008. Two-dimensional mapping of photopigment distribution and activity of *Chloroflexus*-like bacteria in a hypersaline microbial mat. FEMS Microbiol. Ecol. 65 (3), 434–448.

Baleizao, C., Nagl, S., Schäferling, M., Berberan-Santos, M.N., Wolfbeis, O.S., 2008. Dual fluorescence sensor for trace oxygen and temperature with unmatched range and sensitivity. Anal. Chem. 80 (16), 6449–6457.

Behrens, J.W., Stahl, H.J., Steffensen, J.F., Glud, R.N., 2007. Oxygen dynamics around buried lesser sandeels *Ammodytes tobianus*(Linnaeus 1785: mode of ventilation and oxygen requirements. J. Exp. Biol. 210 (6), 1006–1014.

Belding, S.R., Baron, R., Dickinson, E.J.F., Compton, R.G., 2009. Modeling diffusion effects for a stepwise two-electron reduction process at a microelectrode: study of the reduction of para-quaterphenyl in tetrahydrofuran and inference of fast comproportionation of the dianion with the neutral parent molecule. J. Phys. Chem. 113 (36), 16042–16050.

Bittig, H.C., Körtzinger, A., Neill, C., van Ooijen, E., Plant, J.N., Hahn, J., Johnson, K.S., Yang, B., Emerson, S.R., 2018. Oxygen optode sensors: principle, characterization, calibration, and application in the ocean. Front. Mar. Sci. (429), 4.

Blossfeld, S., 2013. Light for the dark side of plant life:—Planar optodes visualizing rhizosphere processes. Plant Soil 369 (1–2), 29–32.

Blossfeld, S., Perriguey, J., Sterckeman, T., Morel, J.-L., Lösch, R., 2010. Rhizosphere pH dynamics in trace-metal-contaminated soils, monitored with planar pH optodes. Plant Soil 330 (1–2), 173–184.

Blossfeld, S., Gansert, D., Thiele, B., Kuhn, A.J., Lösch, R., 2011. The dynamics of oxygen concentration, pH value, and organic acids in the rhizosphere of *Juncus* spp. Soil Biol. Biochem. 43 (6), 1186–1197.

Blossfeld, S., Schreiber, C.M., Liebsch, G., Kuhn, A.J., Hinsinger, P., 2013. Quantitative imaging of rhizosphere pH and CO_2 dynamics with planar optodes. Ann. Bot. 112 (2), 267–276.

Borer, B., Tecon, R., Or, D., 2018. Spatial organization of bacterial populations in response to oxygen and carbon counter-gradients in pore networks. Nat. Commun. 9 (1), 769.

Borisov, S.M., Klimant, I., 2007. Ultrabright oxygen optodes based on cyclometalated iridium(III) coumarin complexes. Anal. Chem. 79 (19), 7501–7509.

Borisov, S.M., Klimant, I., 2008a. Blue LED excitable temperature sensors based on a new europium(III) chelate. J. Fluoresc. 18 (2), 581–589.

Borisov, S.M., Klimant, I., 2008b. Luminescent nanobeads for optical sensing and imaging of dissolved oxygen. Microchim. Acta 164 (1–2), 7–15.

Borisov, S.M., Wolfbeis, O.S., 2006. Temperature-sensitive europium(iii) probes and their use for simultaneous luminescent sensing of temperature and oxygen. Anal. Chem. 78 (14), 5094–5101.

Borisov, S.M., Krause, C., Arain, S., Wolfbeis, O.S., 2006. Composite material for simultaneous and contactless luminescent sensing and imaging of oxygen and carbon dioxide. Adv. Mater. 18 (12), 1511–1516.

Borisov, S.M., Herrod, D.L., Klimant, I., 2009a. Fluorescent poly(styrene-block-vinylpyrrolidone) nanobeads for optical sensing of pH. Sensors Actuators B Chem. 139 (1), 52–58.

Borisov, S.M., Mayr, T., Mistlberger, G., Waich, K., Koren, K., Chojnacki, P., Klimant, I., 2009b. Precipitation as a simple and versatile method for preparation of optical nanochemosensors. Talanta 79 (5), 1322–1330.

Borisov, S.M., Gatterer, K., Bitschnau, B., Klimant, I., 2010. Preparation and characterization of chromium(iii)-activated yttrium aluminum borate: a new thermographic phosphor for optical sensing and imaging at ambient temperatures. J. Phys. Chem. 114 (19), 9118–9124.

Borisov, S.M., Seifner, R., Klimant, I., 2011. A novel planar optical sensor for simultaneous monitoring of oxygen, carbon dioxide, pH and temperature. Anal. Bioanal. Chem. 400 (8), 2463–2474.

Borisov, S.M., Quaranta, M., Klimant, I., 2012. Indicators for Optical Oxygen Sensors, Advances in Chemical Bioanalysis. pp. 1–70.

Borisov, S.M., Fischer, R., Saf, R., Klimant, I., 2014. Exceptional oxygen sensing properties of new blue light-excitable highly luminescent europium(iii) and gadolinium(iii) complexes. Adv. Funct. Mater. 24 (41), 6548–6550.

Bottrell, S.H., Mortimer, R.J.G., Spence, M., Krom, M.D., Clark, J.M., Chapman, P.J., 2007. Insights into redox cycling of sulfur and iron in peatlands using high-resolution diffusive equilibrium thin film (DET) gel probe sampling. Chem. Geol. 244 (3–4), 409–420.

Brendel, P.J., Luther III, G.W., 1995. Development of a gold amalgam voltammetric microelectrode for the determination of dissolved Fe, Mn, O_2, and S(-II) in porewaters of marine and freshwater sediments. Environ. Sci. Technol. 29 (3), 751–761.

Brodersen, K.E., Koren, K., Moßhammer, M., Ralph, P.J., Kühl, M., Santner, J., 2017. Seagrass-mediated phosphorus and iron solubilization in tropical sediments. Environ. Sci. Technol. 51 (24), 14155–14163.

Brodersen, K.E., Siboni, N., Nielsen, D.A., Pernice, M., Ralph, P.J., Seymour, J., Kühl, M., 2018. Seagrass rhizosphere microenvironment alters plant-associated microbial community composition. Environ. Microbiol. 20 (8), 2854–2864.

Buss, W., Shepherd, J.G., Heal, K.V., Mašek, O., 2018. Spatial and temporal microscale pH change at the soil-biochar interface. Geoderma 331, 50–52.

Cao, Z., Zhu, Q., Aller, R.C., Aller, J.Y., 2011. A fluorosensor for two-dimensional measurements of extracellular enzyme activity in marine sediments. Mar. Chem. 123 (1–4), 23–31.

Cao, Z., Zhu, Q., Aller, R.C., Aller, J.Y., Waugh, S., 2013. Seasonal, 2-D sedimentary extracellular enzyme activities and controlling processes in Great Peconic Bay, Long Island. J. Mar. Res. 71 (6), 399–423.

Carraway, E., Demas, J., DeGraff, B., Bacon, J., 1991. Photophysics and photochemistry of oxygen sensors based on luminescent transition-metal complexes. Anal. Chem. 63 (4), 337–342.

Cesbron, F., Metzger, E., Launeau, P., Deflandre, B., Delgard, M.L., Thibault de Chanvalon, A., Geslin, E., Anschutz, P., Jezequel, D., 2014. Simultaneous 2D imaging of dissolved iron and reactive phosphorus in sediment porewaters by thin-film and hyperspectral methods. Environ. Sci. Technol. 48 (5), 2816–2826.

Chatni, M.R., Maier, D.E., Porterfield, D.M., 2009. Evaluation of microparticle materials for enhancing the performance of fluorescence lifetime based optrodes. Sensors Actuators B Chem. 141 (2), 471–477.

Choi, M.M.F., Hawkins, P., 2003. Development of an optical hydrogen sulphide sensor. Sensors Actuators B Chem. 90 (1–3), 211–215.

Christel, W., Zhu, K., Hoefer, C., Kreuzeder, A., Santner, J., Bruun, S., Magid, J., Jensen, L.S., 2016. Spatiotemporal dynamics of phosphorus release, oxygen consumption and greenhouse gas emissions after localised soil amendment with organic fertilisers. Sci.

Total Environ. 554–555, 119–129.
Clarke, J.S., Achterberg, E.P., Connelly, D.P., Schuster, U., Mowlem, M., 2017. Developments in marine pCO_2 measurement technology; towards sustained in situ observations. TrAC Trends Anal. Chem. 88, 53–61.
Courbat, J., Briand, D., Damon-Lacoste, J., Wöllenstein, J., de Rooij, N.F., 2009. Evaluation of pH indicator-based colorimetric films for ammonia detection using optical waveguides. Sensors Actuators B Chem. 143 (1), 62–70.
Davison, W., 2016. Diffusive Gradients in Thin-Films for Environmental Measurements. Cambridge Environmental Chemistry.
Davison, W., Zhang, H., 1994. In situ speciation measurements of trace components in natural waters using thin-film gels. Nature 367 (6463), 546–548.
Davison, W., Grime, G.W., Morgan, J.A.W., Clarke, K., 1991. Distribution of dissolved iron in sediment pore waters at submillimetre resolution. Nature 352 (6333), 323–325.
Davison, W., Fones, G.R., Grime, G.W., 1997. Dissolved metals in surface sediment and a microbial mat at 100-μm resolution. Nature 387 (6636), 885–888.
Delin, S., Strömberg, N., 2011. Imaging-optode measurements of ammonium distribution in soil after different manure amendments. Eur. J. Soil Sci. 62 (2), 295–304.
Demas, J.N., DeGraff, B., Xu, W., 1995. Modeling of luminescence quenching-based sensors: comparison of multisite and nonlinear gas solubility models. Anal. Chem. 67 (8), 1377–1380.
Ding, S., Sun, Q., Xu, D., 2010. Development of the DET technique for high-resolution determination of soluble reactive phosphate profiles in sediment pore waters. Int. J. Environ. Anal. Chem. 90 (14–15), 1130–1138.
Ding, S., Chen, M., Cui, J., Wang, D., Lin, J., Zhang, C., Tsang, D.C.W., 2018. Reactivation of phosphorus in sediments after calcium-rich mineral capping: implication for revising the laboratory testing scheme for immobilization efficiency. Chem. Eng. J. 331, 720–728.
Dmitriev, R.I., Papkovsky, D.B., 2018. Quenched-Phosphorescence Detection of Molecular Oxygen: Applications in Life Sciences. 11 Royal Society of Chemistry.
Dmitriev, R.I., Kondrashina, A.V., Koren, K., Klimant, I., Zhdanov, A.V., Pakan, J.M.P., McDermott, K.W., Papkovsky, D.B., 2014. Small molecule phosphorescent probes for O_2 imaging in 3D tissue models. Biomaterials Sci. 2 (6), 853–866.
Ehgartner, J., Wiltsche, H., Borisov, S.M., Mayr, T., 2014. Low cost referenced luminescent imaging of oxygen and pH with a 2-CCD colour near infrared camera. Analyst 139 (19), 4924–4933.
Elberling, B., Askaer, L., Jorgensen, C.J., Joensen, H.P., Kuhl, M., Glud, R.N., Lauritsen, F.R., 2011. Linking soil O_2, CO_2, and CH_4 concentrations in a Wetland soil: implications for CO_2 and CH_4 fluxes. Environ. Sci. Technol. 45 (8), 3393–3399.
Elgetti Brodersen, K., Koren, K., Lichtenberg, M., Kuhl, M., 2016. Nanoparticle-based measurements of pH and O_2 dynamics in the rhizosphere of *Zostera marina* L.: effects of temperature elevation and light-dark transitions. Plant Cell Environ. 39 (7), 1619–1630.
Faget, M., Blossfeld, S., von Gillhaussen, P., Schurr, U., Temperton, V.M., 2013. Disentangling who is who during rhizosphere acidification in root interactions: combining fluorescence with optode techniques. Front. Plant Sci. 4, 392.
Fan, Y., Zhu, Q., Aller, R.C., Rhoads, D.C., 2011. An in situ multispectral imaging system for planar optodes in sediments: examples of high-resolution seasonal patterns of pH. Aquat. Geochem. 17 (4–5), 457–471.
Fischer, J.P., Wenzhöfer, F., 2010. A novel planar optode setup for concurrent oxygen and light field imaging: application to a benthic phototrophic community. Limnol. Oceanogr. Methods 8 (6), 254–268.
Franke, R., Holst, G.A., 2015. Frequency-Domain Fluorescence Lifetime Imaging System (Pco. Flim) Based on a in-Pixel Dual Tap Control CMOS Image Sensor, Imaging, Manipulation, and Analysis of Biomolecules, Cells, and Tissues XIII. International Society for Optics and Photonics, pp. 93281K.
Franke, U., Polerecky, L., Precht, E., Huettel, M., 2006. Wave tank study of particulate organic matter degradation in permeable sediments. Limnol. Oceanogr. 51 (2), 1084–1096.
Frederiksen, M.S., Glud, R.N., 2006. Oxygen dynamics in the rhizosphere of *Zostera marina*: a two-dimensional planar optode study. Limnol. Oceanogr. 51 (2), 1072–1083.
Gambrell, R.P., Wiesepape, J.B., Patrick, W.H., Duff, M.C., 1991. The effects of pH, redox, and salinity on metal release from a contaminated sediment. Water Air Soil Pollut. 57 (1), 359–367.
Gao, Y., Leermakers, M., Gabelle, C., Divis, P., Billon, G., Ouddane, B., Fischer, J.C., Wartel, M., Baeyens, W., 2006. High-resolution profiles of trace metals in the pore waters of riverine sediment assessed by DET and DGT. Sci. Total Environ. 362 (1–3), 266–277.
Ge, Y., Bai, G., Stoerger, V., Schnable, J.C., 2016. Temporal dynamics of maize plant growth, water use, and leaf water content using automated high throughput RGB and hyperspectral imaging. Comput. Electron. Agric. 127, 625–632.
Gehmert, S., Geis, S., Lamby, P., Roll, C., Braumandl, U., Hidayat, M., Sultan, M., Fuechtmeier, B., Jung, E.M., Prantl, L., 2011. Evaluation of hyperbaric oxygen therapy for free flaps using planar optical oxygen sensors. Preliminary results. Clin. Hemorheol. Microcirc. 48 (1), 75–79.
Glud, R.N., 2008. Oxygen dynamics of marine sediments. Mar. Biol. Res. 4 (4), 243–289.
Glud, R.N., Ramsing, N.B., Gundersen, J.K., Klimant, I., 1996. Planar optrodes:a new tool for fine scale measurements of two-dimensional O_2 distribution in benthic communities. Mar. Ecol. Prog. Ser. 140 (1–3), 217–226.
Glud, R.N., Santegoeds, C.M., De Beer, D., Kohls, O., Ramsing, N.B., 1998. Oxygen dynamics at the base of a biofilm studied with planar optodes. Aquat. Microb. Ecol. 14 (3), 223–233.
Glud, R.N., Kühl, M., Kohls, O., Ramsing, N.B., 1999. Heterogeneity of oxygen production and consumption in a photosynthetic microbial mat as studied by planar optodes. J. Phycol. 35 (2), 270–279.
Glud, R.N., Tengberg, A., Kühl, M., Klimant, I., Holst, G., 2001. An in situ instrument for planar O_2 optode measurements at benthic interfaces. Limnol. Oceanogr. 46 (8), 2073–2080.
Glud, R.N., Grossart, H.-P., Larsen, M., Tang, K.W., Arendt, K.E., Rysgaard, S., Thamdrup, B., Gissel Nielsen, T., 2015. Copepod carcasses as microbial hot spots for pelagic denitrification. Limnol. Oceanogr. 60 (6), 2026–2036.
Glud, R.N., Berg, P., Stahl, H., Hume, A., Larsen, M., Eyre, B.D., Cook, P.L.M., 2016. Benthic carbon mineralization and nutrient turnover in a Scottish sea loch: an integrative in situ study. Aquat. Geochem. 22 (5–6), 443–467.
Grauw, C.J., Gerritsen, H.C., 2001. Multiple time-gate module for fluorescence lifetime imaging. Appl. Spectrosc. 55 (6), 670–678.
Gryczynski, I., Malicka, J., Holder, E., DiCesare, N., Lakowicz, J.R., 2003. Effects of metallic silver particles on the emission properties of $[Ru(bpy)_3]^{2+}$. Chem. Phys. Lett. 372 (3–4), 409–414.
Haas, A.F., Gregg, A.K., Smith, J.E., Abieri, M.L., Hatay, M., Rohwer, F., 2013. Visualization of oxygen distribution patterns caused by coral and algae. PeerJ 1, e106.
Hakonen, A., Hulth, S., Dufour, S., 2010. Analytical performance during ratiometric long-term imaging of pH in bioturbated sediments. Talanta 81 (4–5), 1393–1401.
Han, J., Burgess, K., 2009. Fluorescent indicators for intracellular pH. Chem. Rev. 110 (5), 2709–2728.
Han, C., Ren, J., Tang, H., Xu, D., Xie, X., 2016. Quantitative imaging of radial oxygen loss from *Valisneria spiralis* roots with a fluorescent planar optode. Sci. Total Environ. 569–570, 1232–1240.
Han, C., Ren, J., Wang, Z., Tang, H., Xu, D., 2017. A novel hybrid sensor for combined imaging of dissolved oxygen and labile phosphorus flux in sediment and water. Water Res. 108, 179–188.
Hancke, K., Sorell, B.K., Lund-Hansen, L.C., Larsen, M., Hancke, T., Glud, R.N., 2014. Effects of temperature and irradiance on a benthic microalgal community: a combined two-dimensional oxygen and fluorescence imaging approach. Limnol. Oceanogr. 59 (5), 1599–1611.
Hartmann, p, Ziegler, W., 1996. Lifetime imaging of luminescent oxygen sensors based on all-solid-state technology. Anal. Chem. 68 (24), 4512–4514.
He, X., Rechnitz, G.A., 1995. Linear response function for fluorescence-based fiber-optic CO_2 sensors. Anal. Chem. 67 (13), 2264–2268.
Hoefer, C., Santner, J., Borisov, S.M., Wenzel, W.W., Puschenreiter, M., 2017. Integrating chemical imaging of cationic trace metal solutes and pH into a single hydrogel layer. Anal. Chem. Acta 950, 88–97.
Hofmann, J., Meier, R.J., Mahnke, A., Schatz, V., Brackmann, F., Trollmann, R., Bogdan, C., Liebsch, G., Wang, X.D., Wolfbeis, O.S., Jantsch, J., 2013. Ratiometric luminescence 2D in vivo imaging and monitoring of mouse skin oxygenation. Methods Appl. Fluoresc. 1 (4), 045002.
Holst, G., Grunwald, B., 2001. Luminescence lifetime imaging with transparent oxygen optodes. Sensors Actuators B Chem. 74 (1–3), 78–90.
Holst, G., Kohls, O., Klimant, I., König, B., Kühl, M., Richter, T., 1998. A modular luminescence lifetime imaging system for mapping oxygen distribution in biological samples. Sensors Actuators B Chem. 51 (1–3), 163–170.
Hulth, S., Aller, R.C., Pia, E., Erik, S., 2002. A pH plate fluorosensor (optode) for early diagenetic studies of marine sediments. Limnol. Oceanogr. 47 (1), 212–220.
Jensen, S.I., Kuhl, M., Prieme, A., 2007. Different bacterial communities associated with the roots and bulk sediment of the seagrass *Zostera marina*. FEMS Microbiol. Ecol. 62 (1), 108–117.
Jiang, Z., Yu, X., Hao, Y., 2017a. Design and fabrication of a ratiometric planar optode for simultaneous imaging of ph and oxygen. Sensors (Basel) 17 (6), 1316.
Jiang, Z., Yu, X., Zhai, S., Hao, Y., 2017b. Ratiometric dissolved oxygen sensors based on ruthenium complex doped with silver nanoparticles. Sensors (Basel) 17 (3), 548.
Jiang, Z., Chen, J., Du, J., Liu, T., Li, X., Yu, H., Zhang, Q., Hu, Y., Liu, F., Yu, X., Zhou, Z., 2018. Ratiometric optical sensor for high-resolution imaging of pH with low cross-talk. Appl. Opt. 57 (34), 9922–9928.
Jokic, T., Borisov, S.M., Saf, R., Nielsen, D.A., Kuhl, M., Klimant, I., 2012. Highly photostable near-infrared fluorescent pH indicators and sensors based on BF2-chelated tetraarylazadipyrromethene dyes. Anal. Chem. 84 (15), 6723–6730.
Jovanovic, Z., Larsen, M., Organo Quintana, C., Kristensen, E., Glud, R.N., 2014. Oxygen dynamics and porewater transport in sediments inhabited by the invasive polychaete *Marenzelleria viridis*. Mar. Ecol. Prog. Ser. 504, 181–192.
Jovanovic, Z., Pedersen, M., Larsen, M., Kristensen, E., Glud, R.N., 2015. Rhizosphere O_2 dynamics in young *Zostera marina* and *Ruppia maritima*. Mar. Ecol. Prog. Ser. 518, 95–105.
Kermis, H.R., Kostov, Y., Harms, P., Rao, G., 2002. Dual excitation ratiometric fluorescent pH sensor for noninvasive bioprocess monitoring: development and application. Biotechnol. Prog. 18 (5), 1047–1053.
Klatt, J.M., Meyer, S., Hausler, S., Macalady, J.L., de Beer, D., Polerecky, L., 2016. Structure and function of natural sulphide-oxidizing microbial mats under dynamic input of light and chemical energy. ISME J. 10 (4), 921–933.
Klimant, I., Wolfbeis, O.S., 1995. Oxygen-sensitive luminescent materials based on silicone-soluble ruthenium diimine complexes. Anal. Chem. 67 (18), 3160–3166.
Klimant, I., Meyer, V., Kühl, M., 1995. Fiber-optic oxygen microsensors, a new tool in aquatic biology. Limnol. Oceanogr. 40 (6), 1159–1165.
Kolb, H.C., Sharpless, K.B., 2003. The growing impact of click chemistry on drug discovery. Drug Discov. Today 8 (24), 1128–1137.
Konig, B., Kohls, O., Holst, G., Glud, R.N., Kühl, M., 2005. Fabrication and test of sol–gel based planar oxygen optodes for use in aquatic sediments. Mar. Chem. 97 (3–4), 262–276.
Koop-Jakobsen, K., Wenzhöfer, F., 2014. The dynamics of plant-mediated sediment oxygenation in spartina anglica rhizospheres—a planar optode study. Estuar. Coasts 38 (3), 951–963.
Koop-Jakobsen, K., Mueller, P., Meier, R.J., Liebsch, G., Jensen, K., 2018. Plant-sediment interactions in salt marshes – an optode imaging study of O_2, pH, and CO_2 gradients in the rhizosphere. Front. Plant Sci. 9, 541.
Koren, K., Borisov, S.M., Klimant, I., 2012. Stable optical oxygen sensing materials based on click-coupling of fluorinated platinum(II) and palladium(II) porphyrins-A convenient way to eliminate dye migration and leaching. Sensors Actuators B Chem. 169 (5), 173–181.
Koren, K., Hutter, L., Enko, B., Pein, A., Borisov, S.M., Klimant, I., 2013. Tuning the

dynamic range and sensitivity of optical oxygen-sensors by employing differently substituted polystyrene-derivatives. Sensors Actuators B Chem. 176 (100), 344–350.
Koren, K., Brodersen, K.E., Jakobsen, S.L., Kuhl, M., 2015. Optical sensor nanoparticles in artificial sediments–a new tool to visualize O_2 dynamics around the rhizome and roots of seagrasses. J. Environ. Qual. 49 (4), 2286–2292.
Koren, K., Jakobsen, S.L., Kühl, M., 2016. In-vivo imaging of O_2 dynamics on coral surfaces spray-painted with sensor nanoparticles. Sensors Actuators B Chem. 237, 1095–1101.
Koren, K., Mosshammer, M., Scholz, V.V., Borisov, S.M., Holst, G., Kühl, M., 2019. Luminescence lifetime imaging of chemical sensors–a comparison between time-domain and frequency-domain based camera systems. Anal. Chem. 91 (5), 3233–3238.
Kreuzeder, A., Santner, J., Scharsching, V., Oburger, E., Hoefer, C., Hann, S., Wenzel, W.W., 2018. In situ observation of localized, sub-mm scale changes of phosphorus biogeochemistry in the rhizosphere. Plant Soil 424 (1), 573–589.
Kühl, M., 2005. Optical microsensors for analysis of microbial communities. Methods Enzymol. 397, 166–199.
Kuhl, M., Rickelt, L.F., Thar, R., 2007. Combined imaging of bacteria and oxygen in biofilms. Appl. Environ. Microbiol. 73 (19), 6289–6295.
Kuhl, M., Holst, G., Larkum, A.W., Ralph, P.J., 2008. Imaging of oxygen dynamics within the endolithic algal community of the massive coral porites lobata. J. Phycol. 44 (3), 541–550.
Kumari, A., Gupta, K.J., 2017. VisiSens technique to measure internal oxygen and respiration in barley roots. Methods Mol. Biol. 1670, 39–45.
Larsen, M., Borisov, S.M., Grunwald, B., Klimant, I., Glud, R.N., 2011. A simple and inexpensive high resolution color ratiometric planar optode imaging approach: application to oxygen and pH sensing. Limnol. Oceanogr. Methods 9 (9), 348–360.
Larsen, M., Santner, J., Oburger, E., Wenzel, W.W., Glud, R.N., 2015. O_2 dynamics in the rhizosphere of young rice plants (*Oryza sativa* L.) as studied by planar optodes. Plant Soil 390 (1–2), 279–292.
Lehto, N.J., Larsen, M., Zhang, H., Glud, R.N., Davison, W., 2017. A mesocosm study of oxygen and trace metal dynamics in sediment microniches of reactive organic material. Sci. Rep. 7 (1), 11369.
Lenzewski, N., Mueller, P., Meier, R.J., Liebsch, G., Jensen, K., Koop-Jakobsen, K., 2018. Dynamics of oxygen and carbon dioxide in rhizospheres of Lobelia dortmanna – a planar optode study of belowground gas exchange between plants and sediment. New Phytol. 218 (1), 131–141.
Li, C., Ding, S., Yang, L., Wang, Y., Ren, M., Chen, M., Fan, X., Lichtfouse, E., 2019. Diffusive gradients in thin films: devices, materials and applications. Environ. Chem. Lett. 17 (2), 801–831.
Liebsch, G., Klimant, I., Wolfbeis, O.S., 1999. Luminescence lifetime temperature sensing based on sol-gels and poly(acrylonitrile)s dyed with ruthenium metal–ligand complexes. Adv. Mater. 11 (15), 1296–1299.
Liebsch, G., Klimant, I., Frank, B., Holst, G., Wolfbeis, O.S., 2000. Luminescence lifetime imaging of oxygen, pH, and carbon dioxide distribution using optical sensors. Appl. Spectrosc. 54 (4), 548–559.
Liebsch, G., Klimant, I., Krause, C., Wolfbeis, O.S., 2001. Fluorescent imaging of ph with optical sensors using time domain dual lifetime referencing. Anal. Chem. 73 (17), 4354–4363.
Lim, T.S., Lee, J.H., Papautsky, I., 2009. Effect of recess dimensions on performance of the needle-type dissolved oxygen microelectrode sensor. Sensors Actuators B Chem. 141 (1), 50–57.
Lu, H., Jin, Y., Tian, Y., Zhang, W., Holl, M.R., Meldrum, D.R., 2011. New ratiometric optical oxygen and pH dual sensors with three emission colors for measuring photosynthetic activity in *Cyanobacteria*. J. Mater. Chem. 2011 (48), 19293–192301.
Martin, B.C., Bougoure, J., Ryan, M.H., Bennett, W.W., Colmer, T.D., Joyce, N.K., Olsen, Y.S., Kendrick, G.A., 2019. Oxygen loss from seagrass roots coincides with colonisation of sulphide-oxidising cable bacteria and reduces sulphide stress. ISME J. 13 (3), 707–719.
Marzocchi, U., Benelli, S., Larsen, M., Bartoli, M., Glud, R.N., 2019. Spatial heterogeneity and short-term oxygen dynamics in the rhizosphere of *Vallisneria spiralis*: Implications for nutrient cycling. Freshw. Biol. 64 (3), 532–543.
Mayr, T., Borisov, S.M., Abel, T., Enko, B., Waich, K., Mistlberger, G., Klimant, I., 2009. Light harvesting as a simple and versatile way to enhance brightness of luminescent sensors. Anal. Chem. 81 (15), 6541–6545.
Mayr, T., Ungerböck, B., Mistlberger, G., Borisov, S.M., Klimant, I., 2012. A simple method to reduce optical cross-talk effects in chemical imaging with planar optodes. Limnol. Oceanogr. Methods 10 (2), 101–109.
Meier, R.J., Schreml, S., Wang, X.D., Landthaler, M., Babilas, P., Wolfbeis, O.S., 2011. Simultaneous photographing of oxygen and pH in vivo using sensor films. Angew. Chem. Int. Ed. 50 (46), 10893–10896.
Metzger, E., Thibault de Chanvalon, A., Cesbron, F., Barbe, A., Launeau, P., Jezequel, D., Mouret, A., 2016. Simultaneous nitrite/nitrate imagery at millimeter scale through the water-sediment interface. Environ. Sci. Technol. 50 (15), 8188–8195.
Mistlberger, G., Medina-Castillo, A.L., Borisov, S.M., Mayr, T., Fernández-Gutiérrez, A., Fernandez-Sanchez, J.F., Klimant, I., 2010. Mini-emulsion solvent evaporation: a simple and versatile way to magnetic nanosensors. Microchim. Acta 172 (3–4), 299–308.
Moses, J.E., Moorhouse, A.D., 2007. The growing applications of click chemistry. Chem. Soc. Rev. 36 (8), 1249–1262.
Moßhammer, M., Strobl, M., Kühl, M., Klimant, I., Borisov, S.M., Koren, K., 2016. Design and application of an optical sensor for simultaneous imaging of pH and dissolved O_2 with low cross-talk. ACS Sensors 1 (6), 681–687.
Moßhammer, M., Brodersen, K.E., Kühl, M., Koren, K., 2019. Nanoparticle-and microparticle-based luminescence imaging of chemical species and temperature in aquatic systems: a review. Microchim. Acta 186 (2), 126.
Murniati, E., Gross, D., Herlina, H., Hancke, K., Glud, R.N., Lorke, A., 2016. Oxygen imaging at the sediment-water interface using lifetime-based laser induced fluorescence (τLIF) of nano-sized particles. Limnol. Oceanogr. Methods 14 (8), 506–517.
Murphy, E.A.K., Reidenbach, M.A., 2016. Oxygen transport in periodically ventilated polychaete burrows. Mar. Biol. 163 (10), 208.
Nagl, S., Baleizao, C., Borisov, S.M., Schaferling, M., Berberan-Santos, M.N., Wolfbeis, O.S., 2007. Optical sensing and imaging of trace oxygen with record response. Angew. Chem. Int. Ed. 46 (13), 2317–2319.
Nevares, I., Crespo, R., Gonzalez, C., del Alamo-Sanza, M., 2014. Imaging of oxygen transmission in the oak wood of wine barrels using optical sensors and a colour camera. Aust. J. Grape Wine Res. 20 (3), 353–360.
Odaci, D., Gacal, B.N., Gacal, B., Timur, S., Yagci, Y., 2009. Fluorescence sensing of glucose using glucose oxidase modified by PVA-pyrene prepared via “click” chemistry. Biomacromolecules 10 (10), 2928–2934.
Oguri, K., Kitazato, H., Glud, R.N., 2006. Platinum octaetylporphyrin based planar optodes combined with an UV-LED excitation light source: an ideal tool for high-resolution O_2 imaging in O_2 depleted environments. Mar. Chem. 100 (1–2), 95–107.
Ogurtsov, V.I., Papkovsky, D.B., 1998. Selection of modulation frequency of excitation for luminescence lifetime-based oxygen sensors. Sensors Actuators B Chem. 51 (1–3), 377–381.
Pascal, L., Maire, O., Volkenborn, N., Lecroart, P., Bichon, S., de Montaudouin, X., Grémare, A., Deflandre, B., 2016. Influence of the mud shrimp *Upogebia pusilla* (Decapoda: Gebiidea) on solute and porewater exchanges in an intertidal seagrass (*Zostera noltei*) meadow of Arcachon Bay: an experimental assessment. J. Exp. Mar. Biol. Ecol. 477, 69–79.
Pedersen, L.L., Dechesne, A., Smets, B.F., 2015a. A nitrate sensitive planar optode; performance and interferences. Talanta 144, 933–937.
Pedersen, L.L., Smets, B.F., Dechesne, A., 2015b. Measuring biogeochemical heterogeneity at the micro scale in soils and sediments. Soil Biol. Biochem. 90, 122–138.
Peng, H., Stich, M.I., Yu, J., Sun, L.N., Fischer, L.H., Wolfbeis, O.S., 2010. Luminescent Europium(III) nanoparticles for sensing and imaging of temperature in the physiological range. Adv. Mater. 22 (6), 716–719.
Pischedda, L., Poggiale, J.C., Cuny, P., Gilbert, F., 2008. Imaging oxygen distribution in marine sediments. The importance of bioturbation and sediment heterogeneity. Acta Biotheor. 56 (1–2), 123–135.
Pischedda, L., Poggiale, J.-C., Cuny, P., Gilbert, F., 2010. Oxygen distribution heterogeneity related to bioturbation quantified by planar optode imaging. Global Chang. Mank.-Mar. Environ. Interact. 277–282.
Pischedda, L., Cuny, P., Esteves, J.L., Poggiale, J.-C., Gilbert, F., 2011. Spatial oxygen heterogeneity in a *Hediste diversicolor* irrigated burrow. Hydrobiologia 680 (1), 109–124.
Polerecky, L., Hamrle, J., Maccraith, B.D., 2000. Theory of the radiation of dipoles placed within a multilayer system. Appl. Opt. 39 (22), 3968.
Polerecky, L., Franke, U., Werner, U., Grunwald, B., de Beer, D., 2005. High spatial resolution measurement of oxygen consumption rates in permeable sediments. Limnol. Oceanogr. Methods 3 (2), 75–85.
Polerecky, L., Volkenborn, N., Stief, P., 2006. High temporal resolution oxygen imaging in bioirrigated sediments. Environ. Sci. Technol. 40 (18), 5763–5769.
Polerecky, L., Bissett, A., Al-Najjar, M., Faerber, P., Osmers, H., Suci, P.A., Stoodley, P., de Beer, D., 2009a. Modular spectral imaging system for discrimination of pigments in cells and microbial communities. Appl. Environ. Microbiol. 75 (3), 758–771.
Polerecky, L., Klatt, J., Alnajjar, M., de Beer, D., 2009b. Hyperspectral Imaging of Biofilm Growth Dynamics.
Precht, E., Franke, U., Polerecky, L., Huettel, M., 2004. Oxygen dynamics in permeable sediments with wave-driven pore water exchange. Limnol. Oceanogr. 49 (3), 693–705.
Prest, E.I., Staal, M., Kühl, M., van Loosdrecht, M.C.M., Vrouwenvelder, J.S., 2012. Quantitative measurement and visualization of biofilm O_2 consumption rates in membrane filtration systems. J. Membr. Sci. 392–393, 66–75.
Przeslawski, R., Zhu, Q., Aller, R., 2009. Effects of abiotic stressors on infaunal burrowing and associated sediment characteristics. Mar. Ecol. Prog. Ser. 392, 33–42.
Revsbech, N.P., 2005. Analysis of microbial communities with electrochemical microsensors and microscale biosensors. Methods Enzymol. 397, 147.
Rickelt, L.F., Askaer, L., Walpersdorf, E., Elberling, B., Glud, R.N., Kuhl, M., 2013. An optode sensor array for long-term in situ oxygen measurements in soil and sediment. J. Environ. Qual. 42 (4), 1267–1273.
Robertson, D., Welsh, D.T., Teasdale, P.R., 2009. Investigating biogenic heterogeneity in coastal sediments with two-dimensional measurements of iron(II) and sulfide. Environ. Chem. 6 (1).
Rudolph, N., Esser, H.G., Carminati, A., Moradi, A.B., Hilger, A., Kardjilov, N., Nagl, S., Oswald, S.E., 2011. Dynamic oxygen mapping in the root zone by fluorescence dye imaging combined with neutron radiography. J. Soils Sediments 12 (1), 63–74.
Rudolph, N., Voss, S., Moradi, A.B., Nagl, S., Oswald, S.E., 2013. Spatio-temporal mapping of local soil pH changes induced by roots of lupin and soft-rush. Plant Soil 369 (1–2), 669–680.
Rudolph, N., Tötzke, C., Kardjilov, N., Oswald, S.E., 2017. Mapping water, oxygen, and pH dynamics in the rhizosphere of young maize roots. J. Plant Nutr. Soil Sci. 180 (3), 336–346.
Scholz, V.V., Muller, H., Koren, K., Nielsen, L.P., Meckenstock, R.U., 2019. The rhizosphere of aquatic plants is a habitat for cable bacteria. FEMS Microbiol. Ecol. 95 (6).
Schröder, C.R., Weidgans, B.M., Klimant, I., 2005. pH fluorosensors for use in marine systems. Analyst 130 (6), 907–916.
Schröder, C.R., Neurauter, G., Klimant, I., 2007a. Luminescent dual sensor for time-resolved imaging of pCO_2 and pO_2 in aquatic systems. Microchim. Acta 158 (3–4), 205–218.
Schröder, C.R., Polerecky, L., Klimant, I., 2007b. Time-resolved pH/pO_2 mapping with luminescent hybrid sensors. Anal. Chem. 79 (1), 60–70.
Song, A., Parus, S., Kopelman, R., 1997. High-performance fiber-optic pH microsensors for practical physiological measurements using a dual-emission sensitive dye. Anal. Chem. 69 (5), 863–867.
Song, D.H., Kim, H.D., Kim, K.C., 2011. Measurement of dissolved oxygen concentration field in a microchannel using PtOEP/PS film. J. Vis. 14 (3), 295–304.
Song, D.H., Kim, H.D., Kim, K.C., 2012. Dissolved oxygen concentration field measurement in micro-scale water flows using PtOEP/PS film sensor. Opt. Lasers Eng. 50 (1), 74–81.

Soto Neira, J., Zhu, Q., Aller, R.C., 2011. A new spectrophotometric method to quantify dissolved manganese in marine pore waters. Mar. Chem. 127 (1–4), 56–63.
Soto Neira, J., Zhu, Q., Aller, R.C., 2013a. Application of Planar Optical Sensor for In-Situ Measurement of Multi-Dimensional Distributions of Mn(II) and Fe(II) in Marine Sediment. Chemical Oceanography Gordon Research Conference.
Soto Neira, J., Zhu, Q., Aller, R.C., 2013b. New Planar Optical Sensor for Measuring 2-D Manganese Distributions in Marine Sediments. ASLO.
Staal, M., Borisov, S.M., Rickelt, L.F., Klimant, I., Kuhl, M., 2011a. Ultrabright planar optodes for luminescence life-time based microscopic imaging of O_2 dynamics in biofilms. J. Microbiol. Methods 85 (1), 67–74.
Staal, M., Prest, E.I., Vrouwenvelder, J.S., Rickelt, L.F., Kuhl, M., 2011b. A simple optode based method for imaging O_2 distribution and dynamics in tap water biofilms. Water Res. 45 (16), 5027–5037.
Stahl, H., Glud, A., Schröder, C.R., Klimant, I., Tengberg, A., Glud, R.N., 2006. Time-resolved pH imaging in marine sediments with a luminescent planar optode. Limnol. Oceanogr. Methods 4 (4), 336–345.
Stahl, H., Warnken, K.W., Sochaczewski, L., Glud, R.N., Davison, W., Zhang, H., 2012. A combined sensor for simultaneous high resolution 2-D imaging of oxygen and trace metals fluxes. Limnol. Oceanogr. Methods 10 (5), 389–401.
Stich, M.I.J., Nagl, S., Wolfbeis, O.S., Henne, U., Schaeferling, M., 2008. A dual luminescent sensor material for simultaneous imaging of pressure and temperature on surfaces. Adv. Funct. Mater. 18 (9), 1399–1406.
Stich, M.I.J., Fischer, L.H., Wolfbeis, O.S., 2010a. Multiple fluorescent chemical sensing and imaging. Chem. Soc. Rev. 39 (8), 3102–3114.
Stich, M.I.J., Schäferling, M., Wolfbeis, O.S., 2010b. Multicolor fluorescent and permeation-selective microbeads enable simultaneous sensing of pH, oxygen, and temperature. Adv. Mater. 21 (22), 2216–2220.
Stockdale, A., Davison, W., Zhang, H., 2009. Micro-scale biogeochemical heterogeneity in sediments: a review of available technology and observed evidence. Earth Sci. Rev. 92 (1–2), 81–97.
Strömberg, N., 2008. Determination of ammonium turnover and flow patterns close to roots using imaging optodes. Environ. Sci. Technol. 42 (5), 1630–1637.
Strömberg, N., Hakonen, A., 2011. Plasmophore sensitized imaging of ammonia release from biological tissues using optodes. Anal. Chem. Acta 704 (1–2), 139–145.
Strömberg, N., Hulth, S., 2001. Ammonium selective fluorosensor based on the principles of coextraction. Anal. Chim. Acta 443 (2), 215–225.
Strömberg, N., Hulth, S., 2003. A fluorescence ratiometric detection scheme for ammonium ions based on the solvent sensitive dye MC 540. Sensors Actuators B Chem. 90 (1–3), 308–318.
Strömberg, N., Hulth, S., 2005. Assessing an imaging ammonium sensor using time correlated pixel-by-pixel calibration. Anal. Chim. Acta 550 (1–2), 61–68.
Strömberg, N., Hulth, S., 2006. Time correlated pixel-by-pixel calibration for quantification and signal quality control during solute imaging. Sensors Actuators B Chem. 115 (1), 263–269.
Strömberg, N., Engelbrektsson, J., Delin, S., 2009a. A high throughput optical system for imaging optodes. Sensors Actuators B Chem. 140 (2), 418–425.
Strömberg, N., Mattsson, E., Hakonen, A., 2009b. An imaging pH optode for cell studies based on covalent attachment of 8-hydroxypyrene-1,3,6-trisulfonate to amino cellulose acetate films. Anal. Chem. Acta 636 (1), 89–94.
Sun, X., Li, Z., Wu, L., Christie, P., Luo, Y., Fornara, D.A., 2019. Root-induced soil acidification and cadmium mobilization in the rhizosphere of *Sedum plumbizincicola*: evidence from a high-resolution imaging study. Plant Soil 436 (1), 267–282.
Thibault de Chanvalon, A., Metzger, E., Mouret, A., Knoery, J., Geslin, E., Meysman, F.J.R., 2017. Two dimensional mapping of iron release in marine sediments at submillimetre scale. Mar. Chem. 191, 34–49.
Tobias, A., Birgit, U., Ingo, K., Torsten, M., 2012. Fast responsive, optical trace level ammonia sensor for environmental monitoring. Chem. Central J. 6 (1), 124.
Tschiersch, H., Liebsch, G., Stangelmayer, A., Borisjuk, L., Rolletschek, H., 2011. Planar Oxygen Sensors for Non Invasive Imaging in Experimental Biology. Microsensors, pp. 2011.
Tschiersch, H., Liebsch, G., Borisjuk, L., Stangelmayer, A., Rolletschek, H., 2012. An imaging method for oxygen distribution, respiration and photosynthesis at a microscopic level of resolution. New Phytol. 196 (3), 926–936.
Van Nguyen, Q., Jensen, L.S., Bol, R., Wu, D., Triolo, J.M., Vazifehkhoran, A.H., Bruun, S., 2017. Biogas digester hydraulic retention time affects oxygen consumption patterns and greenhouse gas emissions after application of digestate to soil. J. Environ. Qual. 46 (5), 1114–1122.
Vieweg, M., Trauth, N., Fleckenstein, J.H., Schmidt, C., 2013. Robust optode-based method for measuring in situ oxygen profiles in gravelly streambeds. Environ. Sci. Technol. 47 (17), 9858–9865.
Volkenborn, N., Polerecky, L., Wethey, D.S., Woodin, S.A., 2010. Oscillatory porewater bioadvection in marine sediments induced by hydraulic activities of *Arenicola marina*. Limnol. Oceanogr. 55 (3), 1231–1247.
Volkenborn, N., Polerecky, L., Wethey, D.S., DeWitt, T.H., Woodin, S.A., 2012. Hydraulic activities by ghost shrimp *Neotrypaea californiensis* induce oxic – anoxic oscillations in sediments. Mar. Ecol. Prog. Ser. 455, 141–156.
Vrouwenvelder, J.S., Prest, E.I.E.C., Kuhl, M., Loosdrecht, M.C.M.V., Staal, M., 2012. Quantitative measurement and visualization of biofilm O_2 consumption rates in-membrane filtration systems. Procedia Eng. 44 (2), 233–234.
Wang, X.D., Wolfbeis, O.S., 2014. Optical methods for sensing and imaging oxygen: materials, spectroscopies and applications. Chem. Soc. Rev. 43 (10), 3666–3761.
Wang, X.D., Meier, R.J., Link, M., Wolfbeis, O.S., 2010. Photographing oxygen distribution. Angew. Chem. Int. Ed. 49 (29), 5027–5029.
Wang, X.D., Meier, R.J., Wolfbeis, O.S., 2012. A fluorophore-doped polymer nanomaterial for referenced imaging of pH and temperature with sub-micrometer resolution. Adv. Funct. Mater. 22 (20), 4202–4207.
Wang, X.D., Wolfbeis, O.S., Meier, R.J., 2013. Luminescent probes and sensors for temperature. Chem. Soc. Rev. 42 (19), 7834–7869.
Warnat, J., Liebsch, G., Stoerr, E.M., Brawanski, A., 2012. Visualisation of cortical pO_2 during an epidural mass lesion in rodents. Acta Neurochir. Suppl. 114, 393–397.
Wei, X., Zhu, Z., Wei, L., Wu, J., Ge, T., 2019. Biogeochemical cycles of key elements in the paddy-rice rhizosphere: microbial mechanisms and coupling processes. Rhizosphere 10, 100145.
Wencel, D., MacCraith, B.D., McDonagh, C., 2009. High performance optical ratiometric sol–gel-based pH sensor. Sensors Actuators B Chem. 139 (1), 208–213.
Wencel, D., Abel, T., McDonagh, C., 2014. Optical chemical pH sensors. Anal. Chem. 86 (1), 15–29.
Wenzel, W.W., Wieshammer, G., Fitz, W.J., Puschenreiter, M., 2001. Novel rhizobox design to assess rhizosphere characteristics at high spatial resolution. Plant Soil 237 (1), 37–45.
Wenzhöfer, F., Glud, R.N., 2004. Small-scale spatial and temporal variability in coastal benthic O_2 dynamics: effects of fauna activity. Limnol. Oceanogr. 49 (5), 1471–1481.
Williams, P.N., Santner, J., Larsen, M., Lehto, N.J., Oburger, E., Wenzel, W., Glud, R.N., Davison, W., Zhang, H., 2014. Localized flux maxima of arsenic, lead, and iron around root apices in flooded lowland rice. J. Environ. Qual. 48 (15), 8498–8506.
Wolfbeis, O.S., 2005. Materials for fluorescence-based optical chemical sensors. J. Mater. Chem. 15 (27–28).
Xing, X., Ding, S., Liu, L., Chen, M., Yan, W., Zhao, L., Zhang, C., 2018. Direct evidence for the enhanced acquisition of phosphorus in the rhizosphere of aquatic plants: a case study on *Vallisneria natans*. Sci. Total Environ. 616–617, 386–396.
Xu, H., Aylott, J.W., Kopelman, R., Miller, T.J., Philbert, M.A., 2001. A real-time ratiometric method for the determination of molecular oxygen inside living cells using sol-gel-based spherical optical nanosensors with applications to rat C6 glioma. Anal. Chem. 73 (17), 4124–4133.
Xu, D., Wu, W., Ding, S., Sun, Q., Zhang, C., 2012. A high-resolution dialysis technique for rapid determination of dissolved reactive phosphate and ferrous iron in pore water of sediments. Sci. Total Environ. 421–422, 245–252.
Yin, H., Zhu, Q., Aller, R.C., 2017. An irreversible planar optical sensor for multi-dimensional measurements of sedimentary H_2S. Mar. Chem. 195, 143–152.
Zelelow, B., Khalil, G.E., Phelan, G., Carlson, B., Gouterman, M., Callis, J.B., Dalton, L.R., 2003. Dual luminophor pressure sensitive paint: II. Lifetime based measurement of pressure and temperature. Sensors Actuators B 96 (1), 304–314.
Zhang, X., Wang, C., 1994. Physical aging and dye diffusion in polysulfone below the glass transition temperature. J. Polym. Sci. B Polym. Phys. 32 (3), 569–572.
Zhang, H., Lei, B., Mai, W., Liu, Y., 2011. Oxygen-sensing materials based on ruthenium (II) complex covalently assembled mesoporous MSU-3 silica. Sensors Actuators B Chem. 160 (1), 677–683.
Zhu, Q., 2019. In situ planar optical sensors for sediment diagenesis study. In: Encyclopedia of Ocean Sciences, pp. 147–156.
Zhu, Q., Aller, R.C., 2010. A rapid response, planar fluorosensor for measuring two-dimensional pCO_2 distributions and dynamics in marine sediments. Limnol. Oceanogr. Methods 8 (7), 326–336.
Zhu, Q., Aller, R.C., 2012. Two-dimensional dissolved ferrous iron distributions in marine sediments as revealed by a novel planar optical sensor. Mar. Chem. 136–137 (2), 14–23.
Zhu, Q., Aller, R.C., 2013. Planar fluorescence sensors for two-dimensional measurements of H_2S distributions and dynamics in sedimentary deposits. Mar. Chem. 157 (12), 49–58.
Zhu, Q., Aller, R.C., Fan, Y., 2005. High-performance planar pH fluorosensor for two-dimensional pH measurements in marine sediment and water. Environ. Sci. Technol. 39 (22), 8906–8911.
Zhu, Q., Aller, R.C., Fan, Y., 2006a. A new ratiometric, planar fluorosensor for measuring high resolution, two-dimensional pCO_2 distributions in marine sediments. Mar. Chem. 101 (1–2), 40–53.
Zhu, Q., Aller, R.C., Fan, Y., 2006b. Two-dimensional pH distributions and dynamics in bioturbated marine sediments. Geochim. Cosmochim. Acta 70 (19), 4933–4949.
Zhu, K., Bruun, S., Larsen, M., Glud, R.N., Jensen, L.S., 2014. Spatial oxygen distribution and nitrous oxide emissions from soil after manure application: a novel approach using planar optodes. J. Environ. Qual. 43 (5), 1809–1812.
Zhu, F., Baker, D., Skommer, J., Sewell, M., Wlodkowic, D., 2015. Real-time 2D visualization of metabolic activities in zebrafish embryos using a microfluidic technology. Cytometry Part A 87 (5), 446–450.